NASA Contractor Report 3063

A New Blade Element Method for Calculating the Performance of High and Intermediate Solidity Axial Flow Fans

Henry V. Borst

CONTRACT NAS2-9079
NOVEMBER 1978

NASA

NASA Contractor Report 3063

A New Blade Element Method for Calculating the Performance of High and Intermediate Solidity Axial Flow Fans

Henry V. Borst
Henry V. Borst & Associates
Wayne, Pennsylvania

Prepared for
Ames Research Center
under Contract NAS2-9079

National Aeronautics
and Space Administration

Scientific and Technical
Information Office

1978

A NEW BLADE ELEMENT METHOD FOR CALCULATING THE PERFORMANCE OF HIGH AND INTERMEDIATE SOLIDITY FANS

Henry V. Borst

SUMMARY

A method is presented to design and predict the performance of axial flow rotors operating in a duct. The same method is suitable for the design of ducted fans and open propellers. The new unified method is based on the blade element approach and the vortex theory for determining the three-dimensional effects, so that two-dimensional airfoil data can be used for determining the resultant force on each blade element. Resolution of this force in the thrust and torque planes and integration allows the total performance of the rotor, fan or propeller to be predicted. Three different methods of analysis, one based on a momentum flow theory; another on the vortex theory of propellers; and a third based on the theory of ducted fans, agree and reduce cascade airfoil data to single line as a function of the loading and induced angle of attack at values of constant inflow angle. The theory applies for any solidity from .01 to over 1 and any blade section camber. The effects of the duct and blade number can be determined so that the procedure applies over the entire range from two-blade open propellers, to ducted helicopter tail rotors, to axial flow compressors with or without guide vanes, and to wind tunnel drive fans. The performance of the rotors can be computed over the range of loadings with good demonstrated accuracy as compared with test results.

INTRODUCTION

The procedures and theories used to calculate the performance of axial flow compressors, ducted fans and open propellers are all different. This is especially true in the case of the methods used for axial flow compressors and propellers. While there are many differences in the detailed characteristics of propellers and axial flow compressors, they both have the same function to provide an increase in pressure downstream, which will result in a thrust force. Thus, the methods of analysis of each type should be based on the same concepts.

With the increased use of axial flow fans for many different applications, such as tail rotors for helicopters and lift fans for V/STOL aircraft, problems in design have developed. The solidity of the fans needed often fell in the range between that where cascade and isolated airfoil theory applied. Thus, in the design and analysis of the fans where a low solidity is encountered outboard on the blade and a high solidity inboard, it is necessary to use two different design approaches. Thus, isolated airfoil theory has been

used to determine the blade performance outboard and cascade theory to find the characteristics inboard. As a result, a region existed on the blade where there is considerable uncertainty.

Because the function of propellers and axial flow fans are the same, a unified method should apply that can be used to calculate the performance of any configuration from a single blade open propeller to a multi-bladed axial flow fan in a duct. An investigation was conducted to develop such a method and the corresponding calculation procedures with the primary purpose of eliminating the uncertainties when low solidity fans are used.

Wallis (ref. 1) studied the "isolated airfoil" method used in the analysis of propellers for use in the design of axial flow compressors. This work depended on empirical corrections to develop corrections to the slope of the lift curve as a function of rotor solidity and air inlet angle. This led to some unrealistic results which could not be explained. While this work is considered to be an important step in the development of a unified method, it did not recognize the true separation of the profile and induced losses that are considered in propeller and wing theory. Thus to apply the "isolated airfoil" concept, further work is required to find the profile and induced loss encountered by axial flow fans. This will permit two-dimensional airfoil data to be used in the design of fans and should eliminate the problems encountered at low and intermediate rotor solidities in the design of ducted helicopter tail rotors, V/STOL lift fans and other fan applications.

SYMBOLS

A	area, m^2 (ft^2)
B	blade number
c	blade chord, cm(ft)
C_D	drag coefficient
C_L	lift coefficient
C_P	power coefficient = $P/\rho n^3 D^5$
C_Q	torque coefficient = $Q/\rho n^2 D^5$
C_T	thrust coefficient = $T/\rho n^2 D^4$
D	drag force, N (lbs)
D	rotor or propeller diameter, cm(ft)
H	total pressure, N/cm^2 $lb/in.^2$

J	advance ratio = V/nD
K(x)	circulation function, (eq. 15)
L	lift force, N (lbs)
m	mass flow
n	rotational speed, rps
P	power, Nm/sec
p	static pressure, N/cm^2 ($lb/in.^2$)
Q	torque, Nm (lb ft)
q	$\frac{1}{2}\rho V^2$, N/m^2 ($lb/in.^2$)
R	rotor or propeller radius, cm(ft)
R'	resultant blade force, N (lb)
r	blade station radius, cm(ft)
T	temperature, K
T	thrust, N (lb)
u	axial induced velocity, m/sec (ft/sec)
V	freestream velocity, m/sec (ft/sec)
v	rotational induced velocity, m/sec (ft/sec)
W	velocity relative to rotor blade, m/sec (ft/sec)
w	displacement velocity, m/sec (ft/sec)
w'	induced velocity, m/sec (ft/sec)
$\bar{w}$	w/V
x	fractional blade radius, r/R
α	angle of attack, deg
α_i	induced angle of attack, deg
β	air angle, angle between air velocity and axial direction, deg

γ $\tan^{-1}(C_D/C_L)$

$\Gamma(x)$ strength of circulation

Δ change

$\varepsilon/\mathcal{M}$ axial loss ratio

η efficiency

ϕ true wind angle, deg

ϕ_o apparent wind angle, deg

$\mathcal{M}$ mass coefficient

ψ blade setting angle rotors, deg

λ pitch of final wake, $(V+w)/\pi nD_w$

ρ fluid density, kg/m^2 ($slugs/ft^3$)

σ solidity, ratio of chord to spacing

Subscripts

c calculated

D duct

i induced

m mean

t test

w wake

o upstream

1 inlet

2 exit rotor

3 stator inlet

4 stator exit

∞ infinity

EXISTING DESIGN METHODS

The existing methods for the design of axial flow compressors, fans and propellers have been developed over the years and are reviewed to provide background for the development of the unified design procedure.

Axial Flow Compressors

The procedures currently used in the design of axial flow compressors depend to a large degree on empirical methods for determining the blade interference loss as well as the profile drag. These methods (ref. 2) depend on extensive test data of airfoil cascades, which give the profile and blade interference drag losses. Cascade data has been run to cover a large number of different types of airfoils, design lift coefficients or camber and a range of solidities. To obtain the data necessary a large matrix of configurations must, and have been, tested (ref. 3).

The application of the cascade data for the design of the axial flow rotors, prerotation vanes and stator vanes depends essentially on determining the turning angle required at each station from the velocity triangle and the power input. So that the required turning angle is obtained, charts have been set up where the best camber can be found for the selected solidity. The blade setting angle required is then determined and the performance calculated. The losses in terms of the diffusion factor are then found as a function of the radial station.

The procedure described above is much more involved when the actual radial flow path through the blades is considered as well as the optimum radial loading and compressibility considerations. Other factors, such as blade stall, effecting surge must also be accounted for in a practical compressor design and evaluation. While the procedures available work extremely well for designing and evaluating the performance of an optimum compressor at a specified condition, difficulty is experienced in calculating the performance at off-design conditions. Also, if the solidity is low or if it is desired to determine the effects of airfoil design variables, problems are encountered in calculating the performance as the basic test data does not cover the required range of operation.

Propellers

The methods used for the design and analysis of propellers depend on the blade element approach where the vortex theory is used to find the three-dimensional flow effects and thus the induced losses. This then allows two-dimensional airfoil data to be used for finding the lift and drag forces at each blade station. By resolving these forces in the thrust and torque planes

and integrating over the blade span, the performance of the propeller is found (ref. 4). This procedure has many advantages as it makes possible the use of any available two-dimensional airfoil data and allows theory to be used for finding the effects of blade number and blade load distribution. This is similar to wing analysis where theory is used to find the losses due to three-dimensional effects.

The vortex theory is used to find the induced losses and the equivalent two-dimensional flow condition. This theory was developed by Goldstein (ref. 5) and was extended by Theodorsen (ref. 6) and others (ref. 7 & 8). It depends on the concept of an optimum load distribution and the so-called rigid wake concept. This theory has proven very effective for calculating the effects of blade number and predicting the induced losses. The application of the theory is given later in this report.

Ducted Propellers

The theory of propellers has been extended to include the effects of enclosing the propeller or rotor with a duct having a finite length (refs. 9 through 11). This theory allows the calculation of the three-dimensional effects of the rotor and duct. As a result, equivalent two-dimensional flow conditions are found so that two-dimensional airfoil data can be used to find the operating lift and drag characteristics, the induced losses and, therefore, the performance. The theory depends on the concept of the optimum load distribution for finding the losses and requires finding the vortex load distribution of the duct to satisfy the condition of the rigid wake. In finding the equivalent two-dimensional flow conditions at each station of the rotor, the velocity induced by the duct and the rotor must be determined. In application, this theory is similar to that of the open propeller and has the same advantages.

BASIC APPROACH

The blade element approach used for analyzing propellers and ducted fans has proven to be very effective in providing a means for determining the best design configuration and its corresponding performance. It has given the designer the source of the losses and, therefore, a means for correcting the problem. With the vortex theory for calculating the induced losses, the effects of blade number can easily be determined and this has thus eliminated the need for conducting extensive tests for evaluating this parameter. For these reasons the blade element approach, using two-dimensional airfoil data or theory for finding the forces at each blade station, has been selected as the basis for the unified design procedure of axial flow compressors, ducted fans and propellers.

THE BLADE ELEMENT THEORY - AXIAL FLOW COMPRESSORS

The blade element method for determining the performance of axial flow compressors depends on determining the equivalent two-dimensional flow conditions so that two-dimensional airfoil data can be used to find the forces on the blade sections. This involves finding the change in the apparent velocity vector as caused by three-dimensional effects. This change in velocity is given by a change in the flow direction relative to the airfoil through an angle of attack α_i, the induced angle of attack. The flow velocity and force diagram for a blade section shown on figure 1 illustrates this velocity change. The lift and drag vectors, determined from the two-dimensional airfoil data at the angle of attack relative to the airfoil section, are normal and parallel to the two-dimensional velocity vector W_m. To find the true three-dimensional lift and drag vectors, the two-dimensional values must be resolved to be normal and parallel to the apparent velocity W_1. This results in an increase of drag as shown on figure 1 relative to the two-dimensional drag. This change between the two- and three-dimensional drag is defined as the induced drag in the same manner as with three-dimensional wings. As seen on figure 1, once the induced angle of attack is known and the two-dimensional values of lift and drag are determined, the thrust and torque forces on the blade section can be determined.

The flow conditions on the blade element of a rotor are generally different from a wing and a propeller with regard to three-dimensional effect. There appears to be no flow about the blade tips and, if an element blade section is considered, no flow between elements. On this basis it would appear that the flow is two-dimensional and the induced drag is zero. However, when a comparison of the flow past a rotor section is made in relation to that of a two-dimensional airfoil, a change is noted that will lead to losses. In conventional theory of a two-dimensional airfoil, the true velocity is that far upstream and the lift and drag vectors are given normal and parallel to this vector. The upwash is considered equal to the downwash past the airfoil and the lift forces are reacted by an increase of pressure transmitted to the stream. When an airfoil section is rotating in a constant area duct, as in the case of an axial flow fan, only the velocity in the axial direction remains constant relative to the section. This is due to continuity considerations assuming an incompressible fluid. Thus, in the axial direction, the lift force is reacted by an increase in pressure. In the rotational direction, the flow is not restrained so there can be an increase of velocity v as is shown on figure 1. The flow condition then becomes different than in a two-dimensional tunnel.

As a result of the production of lift on a rotor, a pressure increase and a change in flow direction are obtained. The change in the flow direction is the result of a three-dimensional condition since the flow is not restricted in the rotational direction. Thus, there is an induced loss as a result of an induced angle of attack change. The amount of this induced loss depends on the proportion of the lift vector in the plane of rotation, which is measured by the turning angle given to the flow $\Delta\beta$ (figure 1). The velocity change in the torque direction is equivalent to a downwash velocity aft of the airfoil.

If half this velocity change takes place at the airfoil and half downstream, then the equivalent two-dimensional flow velocity vector is W_m and the induced angle of attack α_i is equal to half the change in flow angle $\Delta\beta$.

So that two-dimensional airfoil data can be applied for finding the forces on a blade section, it becomes necessary to find the induced angle as a function of the lift and inlet angle. If this can be done, the vast store of two-dimensional wind tunnel airfoil data and theory can be used for the design and analysis of axial flow compressors. This will eliminate the need for cascade airfoil data. Thus, it becomes possible to find the performance with two-dimensional airfoil data, and the effects of Reynolds and Mach numbers can be properly evaluated for the entire range of angle of attack.

Cascade Flow

At any given blade station a series of airfoils with a spacing corresponding to the distance between the rotor blades and operating at an inlet angle corresponding to the operating inlet angle duplicates the flow conditions of a rotor. The relationship between a cascade and a rotor is illustrated on figure 2. A sufficient number of blades must be used in the cascade so that when measurements are made the spacing between blades and the flow conditions at the rotor are duplicated. Further, at the ends of the blades wall interference must be avoided (ref. 2).

Because of the interference between blades of a rotor with a high solidity, the technique for finding the forces on a blade section has been to use cascade airfoil data. These data were used instead of two-dimensional airfoil data so as to properly simulate operating conditions and the blade interference losses. Cascade data are available for a number of different airfoil types (ref. 3). For any given airfoil type the data generally covers a wide range of solidities, camber and inlet angle β_1.

Since the flow conditions of a rotor are duplicated by a cascade and the resulting data contain the sum of the two- and three-dimensional effects, these data were examined to determine if suitable corrections could be found. With such corrections it would be possible to separate out the three-dimensional effects and thus eliminate the need for cascade data.

As shown on figure 2, the flow conditions of a cascade are identical to the rotor; the flow is turned through an angle $\Delta\beta$ and the inlet and exit velocities in each case are W_1 and W_2. Assuming the duct has a constant area in the axial direction, the relative velocity can only change in the rotational direction since continuity must be maintained. As a result, the lift and drag forces on the airfoil are partly reacted by a velocity change and partly by a pressure change. If the flow were allowed to expand, the pressure increase would become a velocity increase. Thus, the pressure rise [illegible] cascade and rotor results from the lift and drag forces, which [illegible] the flow a rotational velocity component.

In the cascade tunnel the forces on the blade sections can be related to the measured turning angle $\Delta\beta$ using the momentum equation, since the mass

flow is known based on the inlet conditions.

Thus, the mass flow in the tunnel is

$$m = \rho A_1 W_1 \qquad (1)$$

By the momentum equation, the mass flow times the change in velocity in the torque direction is equal to the resultant forces on the blade, figure 2.

$$\rho A_1 W_1 \Delta v = R' \cos(\beta_m - \gamma) \qquad (2)$$

The angle β_m is the angle of the mean velocity vector W_m. This velocity vector is considered to be the true velocity of the two-dimensional airfoil section with the lift measured normal to W_m. The lift and drag coefficients are, therefore, based on $q_m = \frac{1}{2}\rho W^2_m$.

The force vector R includes the profile drag force so

$$R = L/\cos\gamma \qquad (3)$$

and

$$\rho A_1 W_1 \Delta v = L \cos(\beta_m - \gamma)/\cos\gamma \qquad (4)$$

At any given station, x, on the rotor the equivalent cascade area is

$$A_1 = \pi x D \Delta x R \cos\beta_1 \qquad (5)$$

Now as indicated on figure 2

$$\sin\beta_1 = \pi n D x / W_1 \quad \text{and} \quad \sin\beta_2 = (\pi n D x - \Delta v)/W_2 \qquad (6)$$

So

$$\Delta v = W_1 \sin\beta_1 - W_2 \sin\beta_2 \qquad (7)$$

Combining equations 4, 5 and 7 and letting

$$L = C_L \frac{\rho}{2} W^2_m \, Bc \Delta x R \quad \text{and} \quad \sigma = \frac{Bc}{\pi x D} \qquad (8)$$

the expression is obtained for the loading parameter σC_L

$$\sigma C_L = \frac{2 \cos\gamma \cos\beta_1 \, W_1^2 (\sin\beta_1 - \cos\beta_1 \tan\beta_2)}{W_m^2 \cos(\beta_m - \gamma)} \qquad (9)$$

Since

$$W_m = W_1 \cos\beta_1 / \cos\beta_m \qquad (10)$$

Equation 9 becomes

$$\sigma C_L = \frac{2 \cos^2\beta_m \cos\gamma (\tan\beta_1 - \tan\beta_2)}{\cos(\beta_m - \gamma)} \quad (11)$$

For the case of zero drag $\gamma = 0$ and equation (11) reduces to

$$\sigma C_L = 2 \cos\beta_m (\tan\beta_1 - \tan\beta_2) \quad (12)$$

Theoretical vs Test Comparisons

Based on the concept that the induced angle α_i

$$\alpha_i = (\beta_1 - \beta_2)/2 \quad (13)$$

and

$$\beta_m = \beta_1 - \alpha_i \quad (14)$$

The variation of σC_L as a function of the induced angle of attack α_i was calculated from equation (12) for inlet angles β_1 of 30, 45, 60 and 70 degrees. The results of these calculations are compared with the cascade test data for NACA 65 series sections operating below the stall on figures 3 through 6. Plotted in this form, the cascade test data is reduced to lines that are only a function of the solidity as the effect of camber is essentially zero. It should be noted that data for variations of design C_L from 0 to 2.7 are included on these plots. To obtain the proper comparison it was necessary to convert the lift coefficient given in reference 2 to the value based on the lift defined normal to W_m and a q corresponding to W_m. The C_L given in reference 3 was defined as normal to the vector W_m with the q based on W_1.

A comparison of the theoretical values of σC_L vs α_i with those measured show generally excellent agreement. The differences bsetween the calculated values assuming zero drag and the test results can easily be due to the difference in drag. For instance if equation (11) is used to find σC_L with finite values of C_D, a reduction in σC_L is obtained. Noted on figure 4 for $\beta_1 = 45^\circ$ are the values of σC_L for $\gamma = 2$, 4, and 6 degrees, which correspond to a lift/drag ratio of 29, 14.3, and 9.5. Thus, the drag vector turns the flow through an additional angle, which can be calculated using equations (11) and (12).

The good agreement between the calculated values of σC_L using equation (12) and the measured quantities from cascade data shows the induced angle is a reliable measure of the three-dimensional effects. This would indicate that two-dimensional airfoil data can be corrected to apply at solidities up to at least 1.25 and that the blade element theory can be applied to calculate the performance of an axial flow compressor. Since the blade element theory is used to calculate the performance of propellers with good results, it is reviewed to determine if it is compatible with equation (12) and the cascade test data.

So that the forces can be determined at any blade element on a propeller, it is necessary to find the angle of attack change due to three-dimensional effects. As indicated above, this angle is defined as the induced angle of attack and for propellers must include the change due to tip losses, as well as the change due to blade number and loading. To calculate the induced angle of attack at the propeller, the vortex theory has been used. This theory assumes that at each blade station a vortex is shed in the wake which forms, along with all the shed vortices, a helical vortex sheet. Such a helical vortex sheet is shed by each blade of the propeller and the vortex sheets extend from the propeller blade to infinity. For a propeller operating with an optimum load distribution, the helical sheets will be rigid and move aft relative to the disk with an axial velocity u and a rotational velocity v as illustrated on figure 7. For the purpose of simplifying the solution, an equivalent velocity w is used instead of u and v. The velocity w is referred to as the displacement velocity and with the free stream and rotational velocity components determines the pitch of the shed vortex sheet (ref. 6).

When the propeller has an optimum loading, the displacement velocity is constant with respect to radius in the final wake. This leads to a rigid helical wake of the vortex sheets for the optimum efficiency (ref. 6). This is referred to as a Betz loading for propellers and a vortex-free loading in compressors. Thus for the optimum loading condition, the load is distributed uniformly spanwise as in the case of a wing with an elliptical distribution. The use of the optimum load distribution for determining the inflow conditions of any propeller operating with a non-optimum distribution can only be justified for the design condition where peak efficiency is desired. In this case, the best load distribution is being sought so that conditions do approach the ideal case. In effect, we are assuming that at each blade radius the conditions are independent of the other stations. This is the concept of independence of blade stations.

Vortex Wake

The vortex wake determines the strength and magnitude of the induced velocity vector at each blade station. This allows the determination of the induced angle due to three-dimensional effects and, thus, the conditions for two-dimensional flow. Knowing the equivalent two-dimensional velocity and its direction, the lift and drag of the airfoil can be found from which the torque, power thrust and efficiency is calculated. The characteristics of the final wake are, therefore, of primary importance for finding the operating conditions and the performance of any rotor, fan or propeller.

For any axial flow, rotor vortices are shed at each station due to the change in blade spanwise circulation. These vortices form a vortex sheet or discontinuity, which in an ideal fluid extend to infinity. The potential difference across the vortex sheet or helical surface at a radius x is equal to the strength of the circulation $\Gamma(x)$ at that point. Based on finding the strength of the circulation $\Gamma(x)$ across the helical surface of a given pitch

and blade number, a factor K(x) is defined which allows the determination of the operating C_L for a given or assumed wake condition. Thus, the variation of C_L can be found as a function of the induced angle of attack. This then allows the application of the two-dimensional airfoil data for finding the forces on the blade.

Circulation Function

The circulation function K(x) is determined by the characteristics of the propeller and the condition of operation. Theodorsen defines K(x) by the relationship

$$K(x) = \frac{B\Gamma(x)n}{(V+w)w} \tag{15}$$

The displacement velocity w is not the real axial velocity of the vortices in the wake, but defines the wake helix angle along with the velocity V and the rotational speed πnDx. The circulation function K(x) depends on the blade number, blade station, the helix angle of the wake and the duct configuration. For the case of optimum loading, $w/V = \bar{w}$ = constant, and the condition where the pressure in the wake is equal to the free stream pressure, K(x) has been determined as a function of blade number, station and helix angle for both ducted and open propellers. For the open propeller Theodorsen (ref. 6) measured the potential using the electrical analogy technique, and thus determined K(x). This work has been confirmed by the Goldstein results (ref. 5) and by others (refs. 7 and 8) by direct calculation and was extended by Wright and Gray (refs. 9 and 10) to the case of ducted propellers. In the case of ducted propellers K(x) was determined for conditions in the wake that represent the optimum distribution of load between the rotor and duct.

Properties of K(x)

The term K(x) represents a measure of the mass flow handled by a section of the propeller. When K(x) is integrated over the blade span, a term defined as the mass coefficient is obtained. Thus

$$\mu = 2\int_0^1 K(x)\, x\,dx \tag{16}$$

The mass coefficient times the projected wake area, the corrected displacement velocity and the density represents the mass handled by the propeller in a unit time. Thus, the thrust can be calculated using the momentum equation. In this case, the increased velocity is the displacement velocity w in the final wake.

Thus, the thrust as determined by the conditions in the wake is

$$T = \rho\mu wA\left[V + w\left(\tfrac{1}{2} + \frac{\varepsilon}{\mu}\right)\right] \tag{17}$$

This equation was developed by Theodorsen (ref. 6).

The circulation function at a given blade station increases with blade number and decreases with an increase in the helix angle. For a single rotation open propeller with an infinite number of blades

$$K(x) = \frac{x^2}{x^2+\lambda^2} \tag{18}$$

For a dual rotating propeller K(x) = 1. Thus, the mass handled is defined by the projected helix area and the actual velocity, as in the case of the simple momentum theory. The significance of a single rotation propeller with an infinite number of blades is that this is the upper limit and represents the case where there are no blade or tip losses. In this case, only the rotational losses are found.

The K(x) term can be used to determine the operating lift at any station that corresponds to a wake shape as determined by its angle and blade number. To find the lift or lift coefficient it is necessary to project conditions in the wake, where the pressure corresponds to free stream conditions, back to the rotor. When this is done the equivalent two-dimensional flow conditions are determined. For the propeller, the conditions at the blade are determined approximately from those in the wake by the momentum equations.

The equation for determining the σC_L at any propeller blade station is found using the procedure given by Theodorsen (ref. 6) as follows:

From equation (15) for the circulation function, the ideal circulation at blade station x is

$$\Gamma(x) = \frac{(V+w)w}{Bn} K(x) \tag{19}$$

$$\text{Now } L = \Gamma\rho W = \tfrac{1}{2}\rho W^2 C_L c \tag{20}$$

$$\text{so } \Gamma = \tfrac{1}{2} W C_L c \tag{21}$$

From figure 7 and noticing that the displacement velocity at the propeller is equal approximately to $\frac{1}{2}w$, then the velocity at the blade section equals

$$W = \frac{1}{\sin\phi} (V+\tfrac{1}{2}w)-\tfrac{1}{2}w \sin\phi \tag{22}$$

$$W = \frac{1}{\sin\phi} (V+\tfrac{1}{2}w \cos^2\phi) \tag{23}$$

From equations (21) and (23)

$$\Gamma = \tfrac{1}{2}C_L c \frac{1}{\sin\phi}(V+\tfrac{1}{2}w\cos^2\phi) \tag{24}$$

Thus

$$cC_L = \frac{V+w}{Bn} wK(x)\frac{2\sin\phi}{V+\frac{1}{2}w\cos^2\phi} \tag{25}$$

Letting $\bar{w} = w/V$ and $\sigma = cB/2\pi r$
the equation for the blade loading σC_L for a propeller is

$$\sigma C_L = \frac{1+\bar{w}}{(1+\frac{1}{2}\bar{w})(1+\frac{1}{2}\bar{w}\cos^2\phi)} 2\bar{w}K(x)\frac{\sin^2\phi}{\cos\phi} \tag{26}$$

In equation (26) the K(x) term is a function of the blade number, helix angle in the final wake λ and the radial blade station x. The variation of K(x) with helix angle and x is given on figures 8 through 11 for 2, 3, 4, and 6 blade propellers.

Since the difference between the apparent wind angle ϕ_o and the true wind angle ϕ is the induced angle of attack (figure 7) a relationship exists for finding the operating lift coefficient and, therefore, the forces on the blade element. To do this the lift coefficient calculated from equation (26) must equal the C_L for that of the airfoil at the given blade section, operating at the same angle of attack as found from two-dimensional airfoil data. The two-dimensional airfoil data used is adjusted to consider any change in the slope of the lift curve due to mutual blade interference effects. So,
C_L @ $\alpha = \beta-\phi_o-\alpha_i$ from two-dimensional airfoil data must equal
C_L @ $\phi = \phi_o + \alpha_i$ from equation (26).

Once the operating C_L above has been determined, the profile drag is found from two-dimensional airfoil such as refs. 11 and 12, and the forces can be resolved in the thrust and torque directions as shown on figure 7 to give the equations which are derived in ref. 4.

$$C_T = \int_0^{1.0} \sigma C_L \frac{\pi x}{4} J^2\left[\frac{1+\frac{\bar{w}}{2}(1-\sin^2\phi)}{\sin\phi}\right]^2 (\cos\phi-\tan\gamma\sin\phi)dx \tag{27}$$

$$C_Q = \int_0^{1.0} \sigma C_L \frac{\pi x^2}{8} J^2\left[\frac{1+\frac{\bar{w}}{2}(1-\sin^2\phi)}{\sin\phi}\right]^2 (\sin\phi+\tan\gamma\cos\phi)dx \tag{28}$$

Thus, by solving for dC_T and dC_Q at each blade station as shown above, the total forces on the propeller can be found for any condition.

Rotor in a Duct

A rotor operating in a duct can be treated in the same manner as a propeller for finding the thrust, power required and efficiency. That is, circulation functions K(x) can be found for the distribution where the loading is optimum. In this case, the wake consists of the helical vortex sheets produced by the rotor with a cylindrical sheet produced by the duct. The cylindrical sheet of the duct encloses the vortex sheets of the rotor. This outer sheet must be of sufficient strength to neutralize the radial flow on the blades.

Due to the rotational speed of the blade, the velocity on each blade section increases as a function of radius. This results in a change in loading with radius and the shedding of a vortex element at each blade station. Thus, a vortex sheet is formed by each blade in much the same manner as with a propeller. The distribution of vorticity, however, is different even for the optimum case, as is illustrated on figure 12. As in the case of a propeller, the optimum distribution for peak performance for a ducted rotor occurs when $\bar{w} = w/V$ in the final wake is constant over the effective disk.

Again, as in the case of an open propeller, the key to the calculation of the performance using the blade element method is finding the circulation function K(x) as a function of the wake parameters, helix angle and blade number. This requires extensive calculations with involved computer programs. Based on the above concept of the optimum load distribution, T. Wright and R.B. Gray (refs. 9 through 11) determined the variation of K(x) with blade number and advance ratio as a function of blade radius. The results of these calculations are given on figures 13 through 18 for rotors with 2, 3, 4, 6, 8 and 12 blades. The variation of K(x) for a rotor operating in a duct compared with the open propeller (figures 8 through 10) indicates that higher values of K(x) are generally obtained at any given x and helix angle for the ducted configuration (figure 12). Comparison of the K(x) for rotors operating in a duct having 8 and 12 blades indicates little difference in K(x) compared with that for an infinite number of blades, equation (18).

The circulation function for a rotor operating in a duct can also be used to find the operating value of C_L. Since, however, K(x) is known for the equivalent helix angle in the final wake, a means must be found to convert the conditions in the final wake to those at the rotor. Then the equivalent two-dimensional airfoil operating conditions can be found, along with C_L and C_D, to allow the application of the blade element method of analysis.

The conversion of the flow conditions in the final wake to rotor will allow the use of the circulation function K(x) for finding C_L and α_i. To make this conversion consider the velocity diagram of a rotor operating in a constant area duct. For convenience in this development the usual axial flow compressor notation will be used. Consider a rotor with an infinite number of blades operating in a constant area duct in an incompressible fluid. Let β_1 be the entrance angle (figure 19). The rotor imparts a rotational velocity component v to the fluid as a result of the power imput. The velocity in the axial direction remains equal to the upstream value V, due to continuity with the force component of the lift developed on the airfoil reacting into a pressure increase. Thus, aft of rotor there is a pressure increase and the development of a rotational velocity component.

Relative to the rotor the inlet velocity is W_1 and the exit velocity is W_2, β_2 being the exit angle. The mean velocity relative to the rotor is W_m, which represents the equivalent two-dimensional conditions, as the upwash is assumed to equal the downwash. Thus, the lift coefficient is defined based on a q corresponding to W_m and is normal to W_m.

At the exit of the duct, the pressure increase aft of the rotor can no longer be supported and is converted to a velocity increase u' when the pressure decreases to the ambient pressure p_o. The resulting axial velocity increase in the wake is equal to u and is determined from Bernoulli's and the continuity equations. Thus, based on the notation given on figure 19

$$H_o = H_1,\ H_2 = H_3;\quad T/A = H_3 - H_o \tag{29}$$

By continuity

$$\rho A_1 V_o = \rho A_2 V_o = \rho A_3 V_3 = \rho A_3 (V_o + u)$$

$$D_2/D_3 = \sqrt{\frac{V_o + u}{V_o}} = (1 + \bar{u})^{\frac{1}{2}} \tag{30}$$

where

$$\bar{u} = u/V$$

The axial velocity increase in the wake u combined with the rotational velocity v determines the pitch of the rigid vortices in the final wake when combined with the forward and rotational vectors (figure 19). The apparent velocity vector w, the displacement velocity, describes the effective pitch of the wake as in the case of propellers (ref. 6). Even though the diameter of the wake is less than that of the duct, the rotational velocity πnDx remains constant between the wake and the rotor by the law of the conservation of angular momentum. Based on this concept, the Theodorsen procedure can now be used to calculate σC_L for any blade station of a ducted fan knowing the conditions in the final wake.

The circulation function K(x) relates to the strength of the circulation Γ. Thus, from equation (15)

$$\Gamma = \frac{K(x)(V+w)w}{Bn} \tag{31}$$

Since the circulation will not change between the rotor and the final wake

$$\Gamma = \tfrac{1}{2} W_m \, cC_L \tag{32}$$

From equations (31) and (32) and the definition $\sigma = Bc/(\pi xD)$

$$\sigma C_L = \frac{2K(x)(1+\bar{w})w}{\tan\beta_1 W_m} \tag{33}$$

From equation (18) the circulation function for an infinite number of blades is and can be written as

$$K(x) = \frac{x^2}{x^2+\lambda^2} = \frac{1}{1+\tan^2\phi_w} = \cos^2\phi_w = \sin^2\beta_{2w}$$

where λ = the pitch of the wake = $V+w/\pi nD_w$

Thus, equation (33) becomes for an infinite blade number

$$\sigma C_L = \frac{2\sin^2\beta_{2w}(1+\bar{w})\bar{w}\,\cos\beta_m}{\tan\beta_1} \tag{34}$$

Based on the velocity triangles at the rotor and in the final wake

$$\tan\beta_2 = \frac{\pi nDx-\Delta v}{V_1} = \frac{\pi nDx}{V_1} - \bar{w}\,\sin\beta_{2w}\cos\beta_{2w}$$

$$\tan\beta_1 = \frac{\pi nDx}{V_1}$$

$$\tan\beta_{2w} = \frac{\pi nDx}{V_1(1+\bar{w})} = \frac{\tan\beta_1}{(1+\bar{w})}$$

and so $$\bar{w} = \frac{\tan\beta_1 - \tan\beta_2}{\sin\beta_{2w}\cos\beta_{2w}}$$

Substituting these relations in equation (34)

$$\sigma C_L = 2\cos\beta_m(\tan\beta_1 - \tan\beta_2)$$

This equation is identical to equation (12) which was derived based on the analysis of the airfoil cascade. Thus, the simplified approach used for calculating σC_L based on momentum analysis of the flow through a cascade compares directly with the propeller and ducted fan theory for the case with an infinite number of blades. Since the test data of the flow through a cascade confirms both equations (12) and, thus, (34), it is now possible to calculate blade interference losses for rotors operating in a duct. These blade interference losses actually correspond to induced losses and are independent of section type and camber. Thus, it becomes possible, using equation (12) or (34), to calculate the induced losses of an axial flow compressor and find the corresponding operating conditions for the application of two-dimensional airfoil data from test or calculation, such as references 12 through 14, to find the profile losses.

Rotor of Finite Blade Number in a Duct

Since the propeller theory, cascade approach and cascade test data agree, the effect of blade number can be determined using equation (12) or (34) modified, using the values of K(x) found by T. Wright and R.B. Gray (refs. 9 through 11). This is done by modifying equation (12) by the ratio of K(x) for the given blade number, figures 13 through 18 by the K(x) for an infinite number of blades. Thus,

$$\sigma C_L = 2\cos(\beta_1-\alpha_i)(\tan\beta_1-\tan(\beta_1-2\alpha_i))\,\frac{K(x)}{K(x)_\infty} \qquad (35)$$

From the above, a method exists where the blade element theory can be used to determine the variation of the loading term σC_L with the induced angle of attack for open propellers and rotors operating in a duct. The theory applies for solidities in the range up to 1.0.

APPLICATION

The excellent agreement of the two theoretical approaches for finding the induced angle of attack as a function of loading σC_L and the further agreement with the cascade test data indicates that the blade element theory can be used to calculate the performance of axial flow fans. This, then, makes it possible to use two-dimensional airfoil data for finding the performance of an axial flow compressor operating in a duct, an open propeller or any axial flow device in between, using the same basic approach. The theory allows the separation and identification of the induced and profile losses and gives the designer the opportunity of optimization to obtain peak performance. The elimination of the need for cascade data makes direct application of two-dimensional airfoil data possible, either from test or from computer calculations.

The blade element theory can be used to find the thrust and torque characteristics of a single rotor with or without prerotation or stator vanes. Knowing the initial flow direction, the turning angle through the rotor can also be determined. To do this it is necessary, as in the case of propellers,

to find the operating lift coefficient at each blade station knowing the relative velocity in the blade setting angle and the airfoil section used. The two-dimensional angle of attack is thus found from the equation

$$\alpha = \beta_1 - \phi - \alpha_i \tag{36}$$

Using equations (35) and (36) and two-dimensional airfoil data, the operating C_L can be found at each blade station. Thus, the C_L at an angle of attack found in equation (34) from two-dimensional airfoil data must agree with the C_L of equation (35), and the induced angle of attack in both equations must be identical. Using two-dimensional airfoil data to find the drag, the resultant force can be found at each blade station. These forces are then resolved into the thrust and torque direction to find the total rotor performance.

Rotor Torque

The equation for finding the torque of a rotor is developed as follows: Consider the lift force on a blade element — it is normal to the mean velocity W_m as shown on figure 1. The addition of the drag force to lift gives the resultant force R which, resolved in the torque direction, gives

$$dQ = rB(\cos(\beta_m - \gamma)) \, dR \tag{37}$$

since $dR = dL/\cos\gamma$

$dL = C_L \frac{\rho}{2} W^2_m \, c \, dr$

$dC_Q = dQ/(\rho n^2 D^5)$

$\sigma = cB/\pi xD$

and from the velocity diagram $W_m/nD = J_D / \cos\beta_m$

and integrating over the blade span, equation (37) becomes

$$C_Q = \int_0^{1.0} \sigma C_L \frac{\pi x^2}{8} \frac{J^2_D}{\cos^2\beta_m} (\cos\beta_m + \sin\beta_m \tan\gamma) dx \tag{38}$$

Rotor Thrust

By resolving the resultant force in the thrust direction, the equation for the thrust coefficient becomes

$$C_T = \int_0^1 \sigma C_L \frac{\pi x}{4} \frac{J^2_D}{\cos^2\beta_m} (\sin\beta_m - \cos\beta_m \tan\gamma) dx \tag{39}$$

In equations (38) and (39) it should be noted that J_D is based on the velocity in the duct ahead of the rotor. Now since

$$C_P = 2\pi C_Q = P/(\rho n^3 D^5) \tag{40}$$

The thrust power of the rotor can be determined for any rotor operating in a duct using the methods described above, as long as the equivalent free stream velocity conditions and fluid density are known.

Duct Induced Velocity

A rotor operating in a duct having a finite shape will be effected by the velocity induced in the rotor plane by the duct. This induced axial velocity is a function of the duct shape, the free stream velocity and rotor thrust. From theory this velocity and duct thrust can be determined, using the procedures developed in references 15 and 16. Computer programs are also available to calculate the inflow velocity of duct (ref. 17).

PREROTATION AND STATOR VANES

The performance of prerotation and stator vanes can be calculated based on the same procedures and theory used to find rotor performance. The objective of the fixed vanes is to eliminate the rotational velocity component in the final wake and thus recover the rotational losses. As a result, the pressure ratio or thrust of the system will be increased.

To calculate the performance of a stator vane, consider the vector diagram, figure 1. The relative inlet velocity vector W_3 is the same as the relative exit velocity of the rotor W_2, figure 1. The relative inlet angle is β_3 and the exit angle β_4. The equivalent two-dimensional velocity vector W^1_m is at an angle β^1_m as shown. So

$$\beta_3 - \alpha_i = \beta^1_m \tag{41}$$

The resultant of the lift and drag vectors dR resolved in the thrust plane gives

$$dT = B\sin(\beta^1_m - \gamma)dR \tag{42}$$

Since $\cos\gamma = L/R$, $dL = C_L \frac{\rho}{2} W^{12}_m \, c \, dr$,

$\sigma = cB/\pi xD$, $J_3 = V_3/nD$

$C_T = T/\rho n^2 D^4$, n = the rotor revolutions per second.

$$\frac{dC_T}{dx} = \sigma C_L \frac{x}{4} \frac{J^2_3}{\cos^2\beta^1_m} (\sin\beta^1_m - \cos\beta^1_m \tan\gamma) \tag{43}$$

Equation (43) integrated across the span gives the thrust recovery of the stator. The effect of prerotation vanes can be determined in a similar manner. In this case, however, the vanes give rotational component to the flow, which results in negative thrust. The rotor removes this rotation with a corresponding thrust increase. The torque developed by the prerotation or stator vanes can be calculated by resolving the forces in the torque plane and finding the torque coefficient in a similar manner. Since the torque developed by the stator vanes is reacted by the duct system, its value is of little interest and is not normally calculated.

COMPRESSIBILITY EFFECTS

The theory used to calculate the performance of axial flow compressors, with or without prerotation and/or stator vanes, is based on incompressible flow. For low pressure ratios, such a theory can be used directly as long as there is an insignificant change in density. With rotors developing high pressure ratio, the effect of the density change will become important and must be considered, especially when determining the exit velocity vectors across each stage. While the overall effects of compressibility are not accounted for in the analysis, their influence will present no difficulty to the analysis.

Equations (38) and (39) can still be used to find the thrust and torque produced by the rotor when operating in a compressible fluid. Then, based on the thrust and torque developed, the pressure and temperature increase aft of the rotor stage can be found. The density ratio across the stage can thus be calculated from the equation from the gas law

$$\rho_1/\rho_2 = (P_1/P_2)(T_2/T_1) \tag{44}$$

In the axial flow direction the continuity equation must be satisfied so, instead of a constant velocity across the rotor stage, the axial velocity becomes

$$V_2 = V_1 \rho_1/\rho_2 \tag{45}$$

This change becomes of interest when it is necessary to determine the characteristics of stator vanes aft of the rotor.

COMPARISON OF TEST VS CALCULATED PERFORMANCE

To determine the accuracy of the blade element method, the calculated performance was compared with test results for rotors operating over a range of conditions. The results of this comparison are given on Tables 1 and 2.

On Table 1 the calculated performance is compared with test for a 6-foot diameter rotor with 15 blades. The blade characteristics of this rotor are given on figure 20. It has a blade solidity varying from 1.06 at the spinner to .35 at the tip, so that it represents the range that is of interest. Comparisons are made for a range of conditions of blade setting angle ϕ and throttle settings, so that the results apply over a range of loadings. The performance was calculated based on a constant inlet velocity ahead of the rotor that was considered to be known. The given rotational speed and blade characteristics then were used to solve equations (35) and (36) to find the operating lift coefficient at each blade station. The thrust and torque were then found from equations (38) and (39). The calculated performance compared with the test results given in reference 18 indicates good agreement over the operating range.[1] Since this rotor was designed for low noise, the tip speed is low. For this reason the effects of compressibility can be expected to be low, and good agreement between test and calculated results would be expected.

Table 2 gives the results of a comparison with a 20-inch diameter run in the NASA compressor facility. The test data and characteristics of this rotor are given in reference 19. The rotor considered has a solidity of .99 inboard and .5 at the tip, and was tested over a wide range of conditions. The results of the test data are presented in compressor notation in terms of total temperature and pressure ratio, and were converted to values of power and thrust for comparison with the calculated data. As before, the rotor performance was calculated using blade element theory; equations (35), (36), (38) and (39); and two-dimensional airfoil data for finding the lift and drag coefficients at each blade section.

The results of this comparison indicate that good accuracy is obtained when the rotor is operating at lift coefficients corresponding to the linear portion of the lift curve. At the upper and lower extremes the accuracy of the calculation method is poor, indicating further work is needed. The accuracy problem at these conditions could be due to the lack of good two-dimensional airfoil data. At the 120% design speed condition the agreement of the calculated performance with that measured is poor. This lack of agreement is due to the compressibility losses that are not considered in the calculations.

---

[1] The accuracy of the calculated performance was improved when the mutual section interference corrections given in reference 1 were used.

DUCTED TAIL ROTOR

The performance of a helicopter tail rotor operating in a duct can also be found using the calculation procedures described in this report. To apply these analysis methods, it is first necessary to determine the velocity just ahead of the rotor as induced by the duct. Since the rotor influences this flow, the velocity must be determined with the rotor operating at its projected thrust level. That is, the pressure rise across the rotor must be considered. For these conditions, the velocity induced by the duct can be calculated using the procedures given in references 15 and 16 or the computer program described in reference 17. Since the methods given in references 15 and 16 apply only for operation at a velocity greater than zero, the method of reference 17 must be used for analysis at the static condition.

The thrust produced by the rotor is then calculated knowing the velocity ahead of the rotor, the rotational speed, and the blade characteristics, using equations (35) and (36) to find the operating C_L at each blade station and then equations (38) and (39) to find thrust and torque. If the velocity ahead of the helicopter is operating at a forward velocity greater than zero, the velocity at each azimuth location must be used for finding the rotor performance, and the results integrated to find the total.

Calculated vs Test Performance

Test data on the performance of a ducted helicopter tail rotor is given in references 20 and 21. For the zero speed condition, the performance of the duct and the rotor was measured using load cells. The rotor thrust was found from the test data using the pressure distribution to estimate the forces generated by the surrounding surfaces and the spinner. For the case where the blade angle is equal to 25 degrees, the ratio of the thrust to power coefficients was calculated to be six percent lower than the measured values. This comparison was made for the case where the power of the test and calculated configurations agree. Based on the methods used to estimate velocity in the plane of the rotor, the accuracy of the comparison of test and calculated performance is considered to be good. Additional test data of ducted tail rotors is needed, however, for evaluation of the calculated method of analysis.

CONCLUDING REMARKS

A unified theory and method of analysis has been developed which is suitable for calculating the performance of axial flow rotors operating with or without a duct. This analysis method applies for the entire range of solidities up to over 1, and so covers the intermediate range between that of propellers and axial flow compressors. It is shown that the analysis procedure eliminates the need for blade cascade data for finding the interference or induced losses, and these losses can be found based on theory. The induced losses are a function of the blade loading, inlet angle, radial station and

blade number. The identification of equivalent two-dimensional flow conditions on a blade element allows the use of two-dimensional airfoil data for finding the profile losses. Thus the designer can use calculated or test two-dimensional airfoil data to find performance, which thus allows the application of advance airfoils without the need to depend on cascade airfoil test data. For a blade section of any solidity the operating lift coefficient required can be determined, which makes possible the selection of the airfoil with the best camber for minimum drag. Since the profile and induced drag losses can be determined at each station, the optimum spanwise loading distribution can be found to minimize the total of these losses and so develop the optimum configuration.

The method of analysis developed for compressors is suitable for finding performance over the entire operating range as well as at the rotor's design conditions. The methods apply for the design of prerotation and stator vanes. Comparisons of the performance of rotors determined by test with that calculated indicated excellent agreement.

RECOMMENDATIONS

Further work is recommended on the new theory of axial flow fans to extend its range of operation. To do this the following areas should be investigated:

1. Analyze the range of loading and operating lift coefficients to find if compressor surge or stall can be explained in terms of the stall of two-dimensional airfoil sections. Develop the necessary corrections to predict compressor surge.

2. Determine the effects of pressure ratio on the lift curve slope based on the analysis given in reference 22. Also, find any limits that may be due to high pressure ratios.

3. Investigate the upper limits of rotor solidity for the application of the unified theory.

4. Through the study of low Reynolds number airfoil data and rotor test data, evaluate the effects of Reynolds number on the efficiency of compressors and the loading at surge.

5. Using high speed rotor test data, develop procedures to account for compressibility effects in calculating rotor performance using the unified theory.

6. Develop the change in K(x) necessary to account for the effects of tip clearance.

7. Investigate means of determining two-dimensional airfoil data from rotor test data to increase the range of data available, especially at the higher design lift coefficients.

8. Conduct studies to determine the possible errors when operating at non-optimum loadings.

9. Using the theory, design a series of optimum rotors and check the predicted performance by test.

REFERENCES

1. Wallis, R.A.; and Aust, F.I.E.: A Rationalized Approach to Blade Element Design, Axial Flow Fans. Institute of Engineers, Australia Conference on Hydraulic and Fluid Mechanics, 1968, Paper No. 2599.

2. Aerodynamic Design of Axial-Flow Compressors. NASA SP-36. N65-23345-362, 1965.

3. Emery, J.C.; et al: Systematic Two-dimensional Cascade Tests of NACA 65-Series Compressor Blades at Low Speeds. NACA TR 1368.

4. Borst, H.V.; et al: Summary of Propeller Design Procedures and Data. Vols. I, II and III. USAAMRDL TR 73-34C, Nov. 1973.

5. Goldstein, Sydney: On the Vortex Theory of Screw Propellers. Proceedings of the Royal Society of London, Ser. AV123, 1929.

6. Theodorsen, T.: Theory of Propellers. McGraw-Hill Book Co., 1948.

7. Kawada, S.: Calculation of Induced Velocity by Helical Vortices and Its Application to Propeller Theory. Report of the Aeronautical Research Institute Tokyo Imperial University Number 172, 1939.

8. Moriya, T.: Calculation Charts of Induced Velocity and Calculation Method of Aerodynamic Characteristics of Propellers. The Journal of the Society of Aeronautical Science of Nippon, Vol. 3, No. 9, Jan. 1936.

9. Wright, T.: Determination of the Design Parameters for Optimum Heavily-Loaded Ducted Fans. Georgia Institute of Technology, Report 69-3, Nov. 1969.

10. Gray, Robin B.; and Wright, Terry: A Vortex Wake Model for Optimum Heavily-Loaded Ducted Fans. Journal of Aircraft, Vol. 7, No. 2, 1970.

11. Wright, Terry: Evaluation of the Design Parameters for Optimum Heavily-Loaded Ducted Fans. Journal of Aircraft, Vol. 7, No. 6, 1970.

12. Stack, John: Tests of Airfoils Designed to Delay the Compressibility Burble. NACA TR 763.

13. Lindsey, W.F.; Stevenson, D.B.; and Daley, Bernard N.: Aerodynamic Characteristics of 24 NACA Series Airfoils at Mach Number Between 0.3 and 0.8. NACA TN 1546.

14. Abbott, Ira H.; von Doenhoff, A.E.; and Stivers, L.S.: Summary of Airfoil Data. Wartime Report No. L-560.

15. Kaskel, A.L.; Ordway, D.E.; Hough, G.R.; and Ritter, A.: A Detailed Numerical Evaluation of Shroud Performance for Finite-Bladed Ducted Propellers. Therm. Report No. TAR-TR639, Dec. 1963.

16. Kaskel, A.L.; and Greenberg, M.D.: A Detailed Numerical Evaluation of Shroud Performance for Finite-Bladed Ducted Propellers Addendum: Compilation of Shroud-Induced Axial Velocity. Therm. Report No. TAR-TR6508, Dec. 1965.

17. Stockman, N.O.; and Button, S.L.: Computer Programs For Calculating the Potential Flow in Propulsion Systems Inlets. NACA TMS-68278, 1973.

18. Page, V. Robert; Eckert, William T.; and Mort, Kenneth W.: An Aerodynamic Investigation of Two 1.83-Meter-Diameter Fan Systems Designed to Drive a Subsonic Wind Tunnel. NASA TM-73,175, Sept. 1977.

19. Osborn, W.M.; and Steinke, R.J.: Performance of a 1.15 Pressure Ratio Axial-Flow Fan Stage With a Blade Solidity of 0.5". NASA TM X-3052.

20. Meier, W.H.; Groth, W.P.; Clark, D.R.; and Verzella, D.: Flight Testing of a Fan-in-Fin Antitorque and Directional Control System and a Collective Force Augmentation System (CFAS). USAAMRDL-TR-75-19, Sikorsky Aircraft Division.

21. Clark, David R.: Aerodynamic Design Rationale for the Fan-in-Fin on the S-67 Helicopter. American Helicopter Society Report, Preprint No. 904, May 1975.

22. Lakshminarayara, B.; and White, M.B.: Airfoil in a Contracting or Diverging Stream. Journal of Aircraft, Vol. 9, No. 5, May 1972.

TABLE 1

CALCULATION OF PERFORMANCE

SUMMARY SHEET

NASA 40x80 ft TUNNEL

Second Rotor

B = 15 D = 6

Spinner = 32"

T Set**	ϕ_t	C_{Pt}	J	η_t	$\Delta\phi_c$	C_{Pc}	η_c	$\Delta\eta$
126	43.2	1.99	2.268	77.6	0	1.675	77.9	
					-2.4	2.063*	77.0	- .6
120	43.2	2.043	2.20	75.3	0	1.750	77.4	
					-2.1	2.087*	77.1	+1.8
110	43.2	2.081		75.0	0	1.881	78.0	
					-1.3	2.057*	76.9	+1.9
100	43.2	1.971	1.775	75.1	0	1.973	76.4	+1.3
90	43.2	1.915	1.658	73.0	0	1.986	75.3	+2.3
80	43.2	1.873	1.579	71.7	0	1.99	74.1	
					+ .74	1.92*	74.9	+3.2
70	43.2	1.761	1.288	67.1	0	1.943	68.1	
					+1.2	1.855	69.7	+2.6
					+2.0	1.798*	70.6	+3.5
120	40.9	2.286	2.299	73.2	0	2.060	77.3	+4.1
					-1.12	2.244*	76.3	+3.4
100	40.9	2.1527	1.8515	73.6	0	2.2129	75.09	+1.5
80	40.9	2.0671	1.5745	69.4	0	2.1966	71.64	+2.24
					+ .6	2.1570	71.56	+2.16
					+1.5	2.0678*	72.95	+3.55
80	52.9	1.2781	1.2824	76.1	0	1.2271	78.72	+2.6
					- .9	1.2943*	78.03	+1.9
70	52.9	1.2241	1.0259	71.1	0	1.2460	73.97	+2.9
60	52.9	1.1824	.9888	73.1	0	1.2428	72.84	-0.3
					+1.08	1.1863*	73.76	+0.7

* Blade setting angle adjusted until calculated power agrees with test within $\pm$ 4%.

** T/Set = throttle setting.

TABLE 2

COMPARISON OF TEST AND CALCULATED

ROTOR PERFORMANCE

Ref. NASA TM X-3052

% Design Speed	Run No.	Test C_P	Test C_T	Cal C_P	Cal C_T	Test/Cal $C_T/C_P/C_T/C_P$	β_1 @.81 R
100	1532	1.837	.4491	1.894	.5838	.7932	43.0
	1400	2.255	.7807	2.237	.7730	1.002	47.0
	1402	2.357	.8664	2.348	.8588	1.005	49.7
	1404	2.393	.9073	2.408	.9211	.9909	52.0
	1405	2.448	.8139	2.392	.9317	.8536	54.6
90	1540	1.859	.4302	1.641	.4733	.8023	41.0
	1411	2.055	.7602	2.184	.7488	1.079	46.7
	1412	2.201	.8445	2.320	.8330	1.068	49.0
	1413	2.309	.9101	2.422	.9144	1.044	51.7
	1415	2.391	.9331	2.423	.9796	.9654	55.4
110	1533	1.725	.4383	2.079	.6778	.7794	44.8
	1534	2.180	.7038	2.232	.7687	.9375	47.0
	1418	2.329	.8524	2.322	.8380	1.0142	49.0
	1420	2.505	.9538	2.406	.9091	1.008	51.7
	1421	2.479	.9300	2.391	.9365	.9579	52.8
	1538	1.827	.4354	2.195	.7444	.7023	46.4
	1537	2.265	.6834	2.303	.8243	.8431	48.5
	1536	2.547	.7964	2.385	.8912	.8367	50.9
	1535	2.643	.8436	2.410	.9463	.8128	53.0

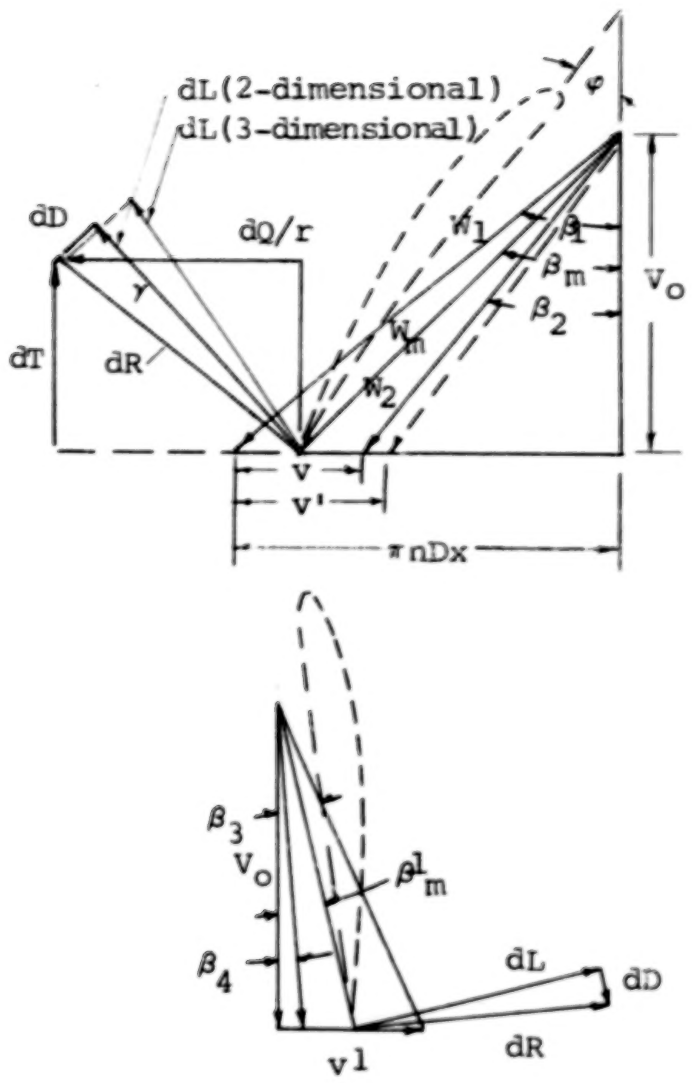

Figure 1. Velocity and force diagrams for rotor and stator blade sections operating in a constant area duct.

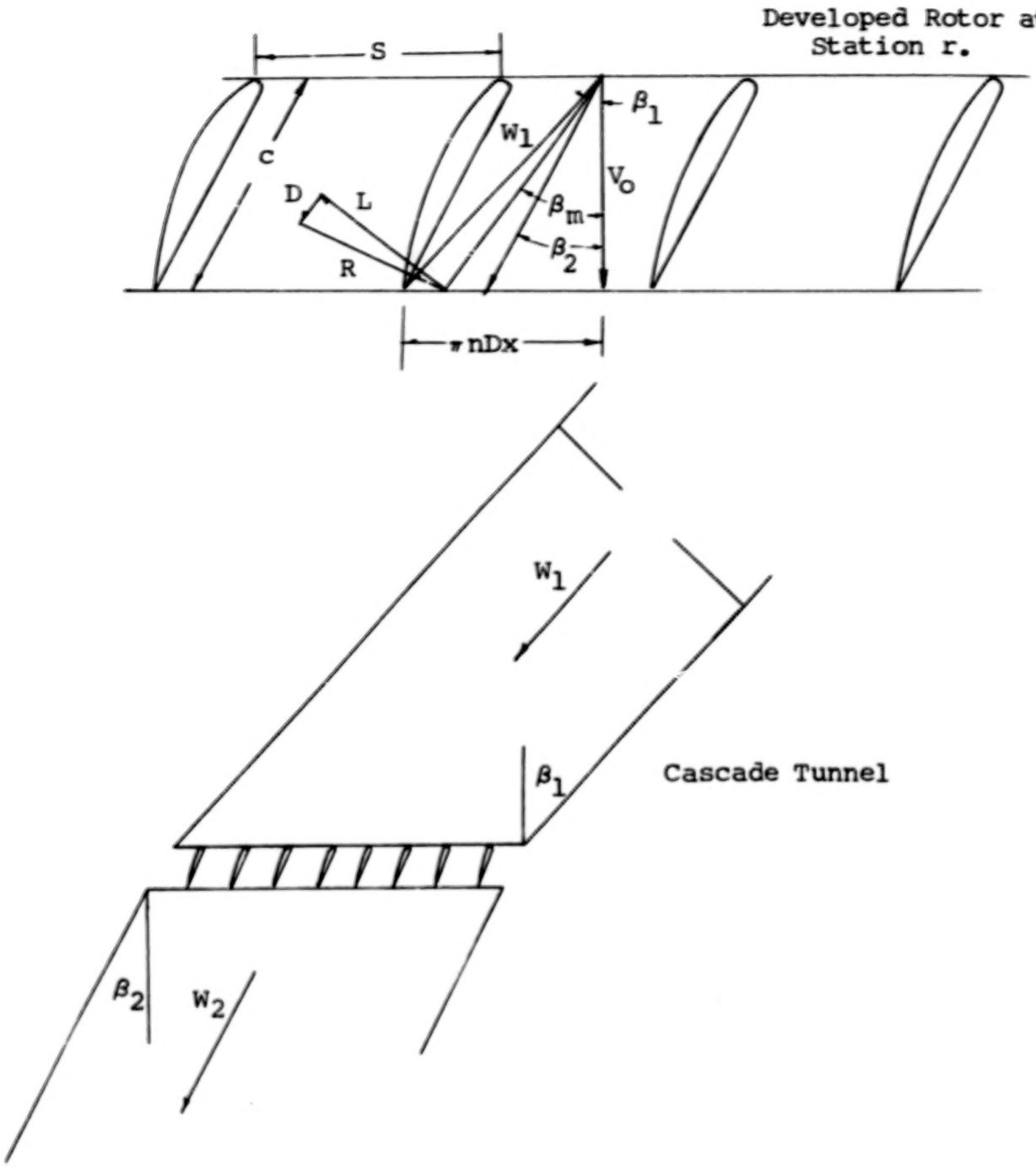

Figure 2. Duplication of the flow through a rotor using a cascade of airfoils.

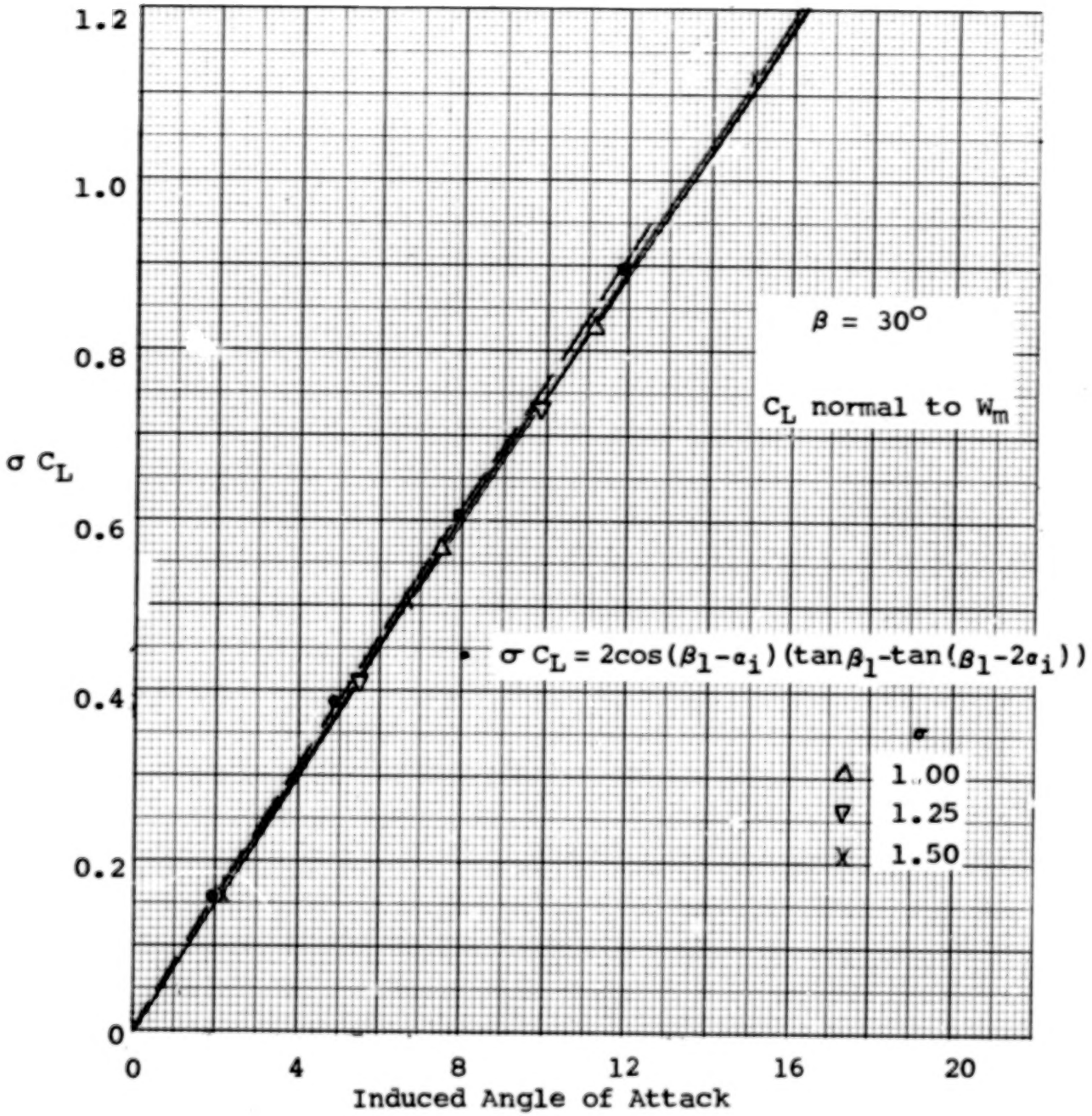

Figure 3. Blade section loading parameter vs induced angle of attack, inlet angle = 30°.

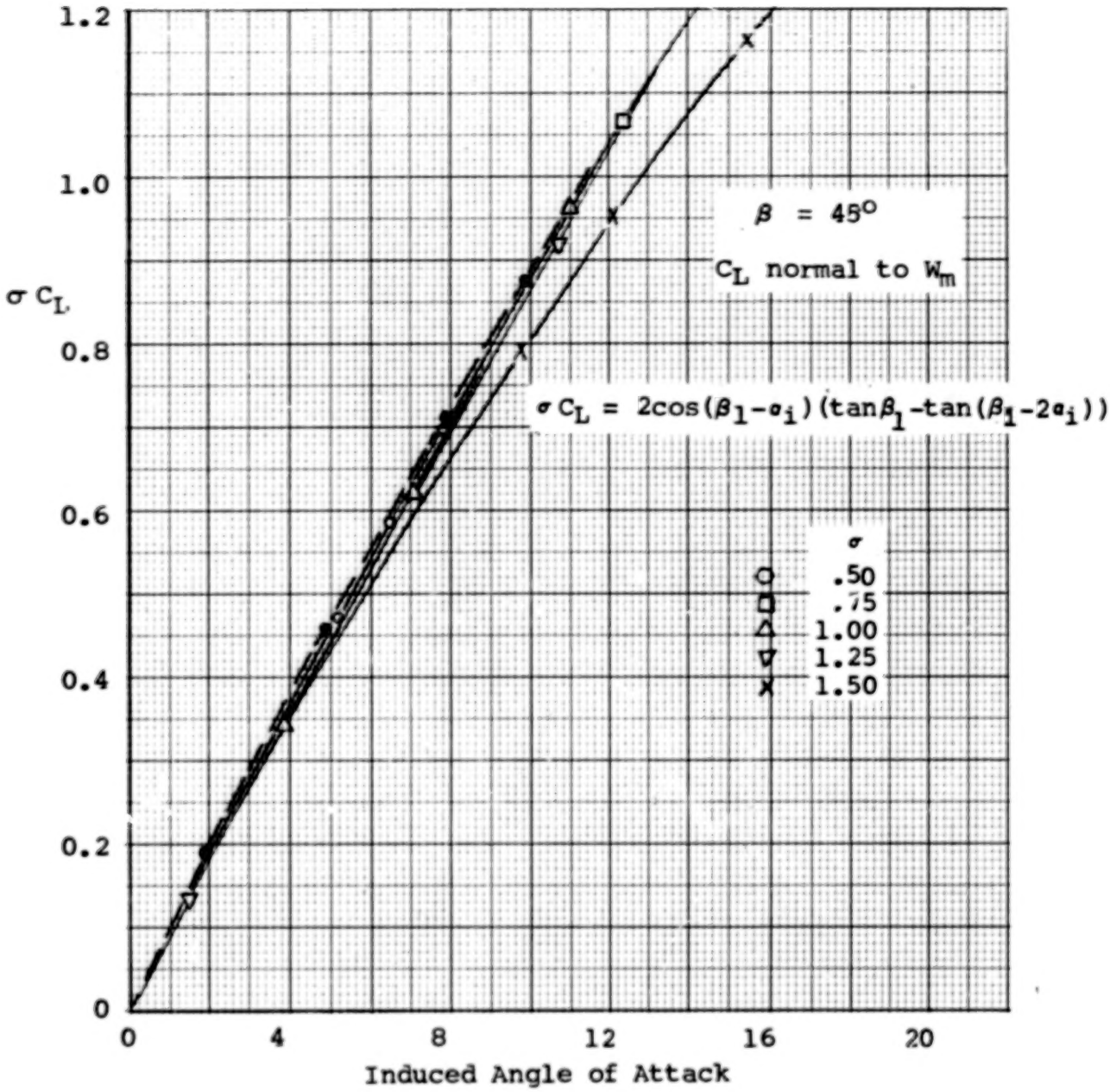

Figure 4. Blade section loading parameter vs induced angle of attack, inlet angle = 45°.

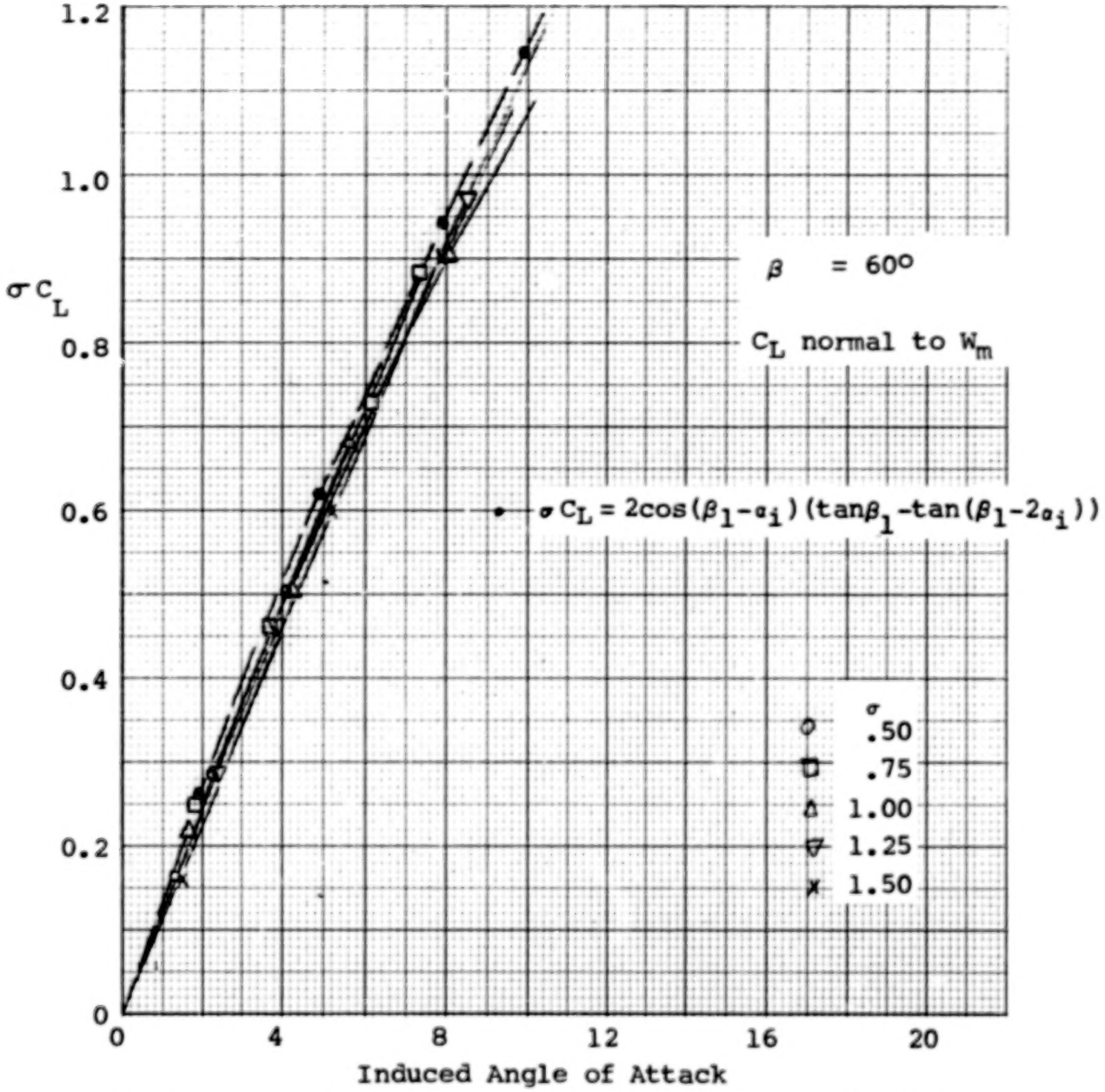

Figure 5. Blade section loading parameter vs induced angle of attack, inlet angle = 60°.

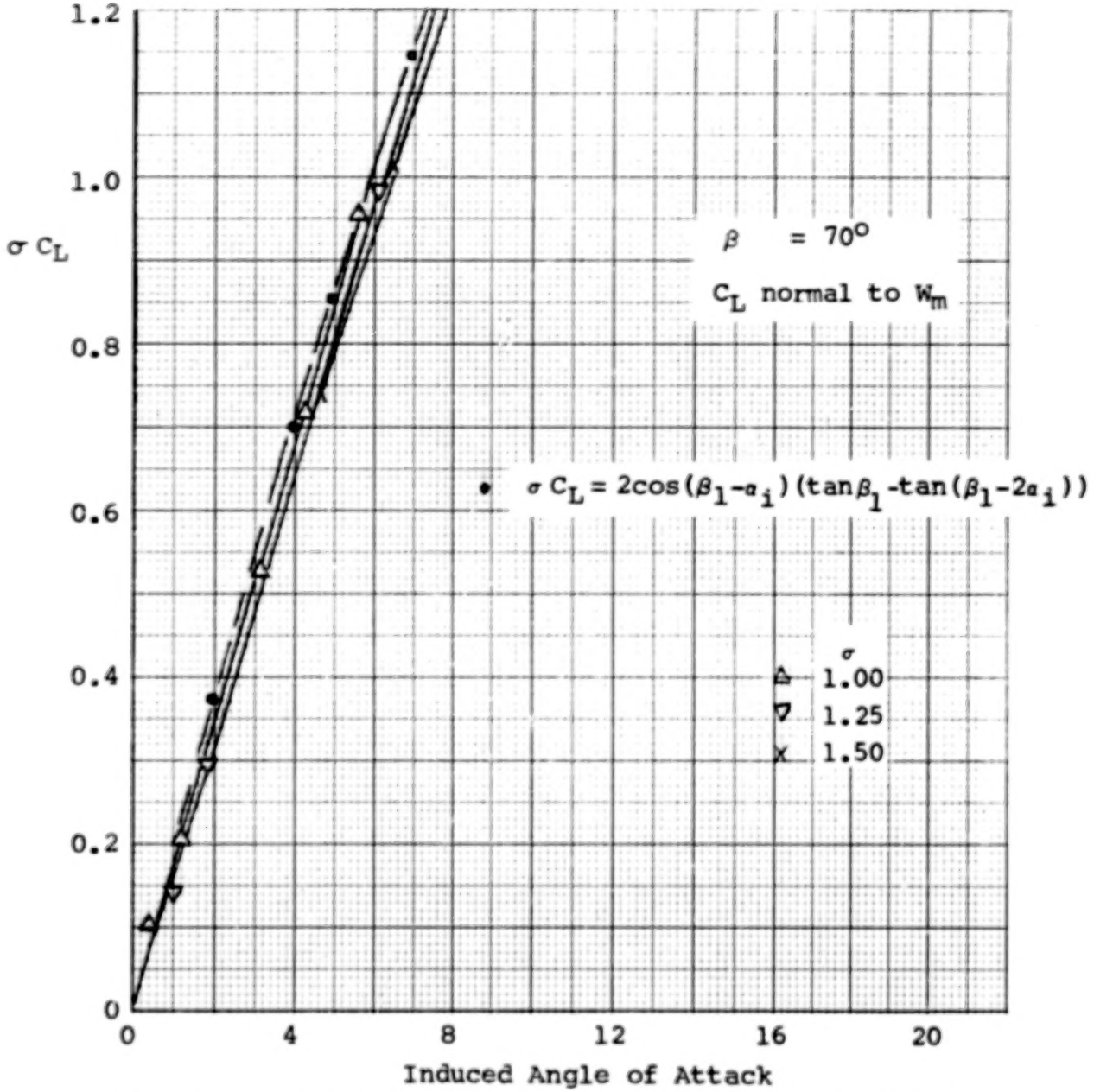

Figure 6. Blade section loading parameter vs induced angle of attack, inlet angle = 70°.

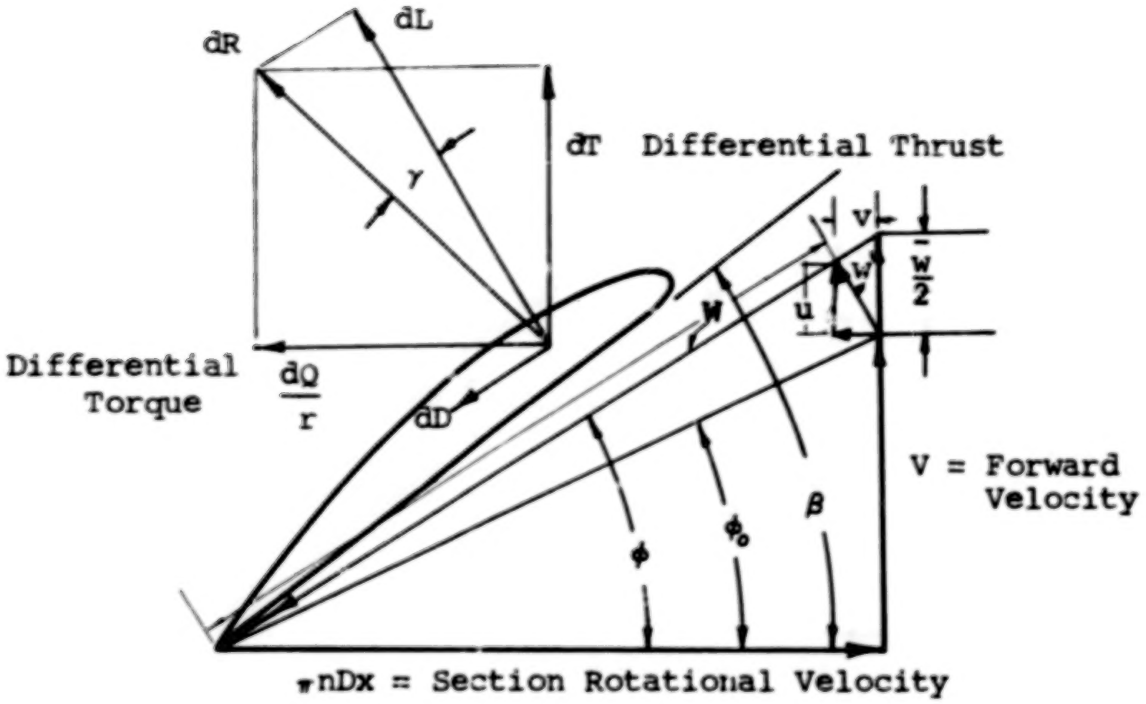

dQ/r = Section Torque
dL = Section Lift
dD = Section Drag
β = Blade Angle
ϕ = True Wind Angle
ϕ_o = Apparent Wind Angle
$\bar{w}/2$ = Displacement Velocity
W = Apparent Velocity
w' = Induced Velocity
w = Axial Inflow Velocity
v = Rotational Inflow Velocity
$\gamma = \tan^{-1} \frac{C_D}{C_L}$

Figure 7. Propeller Velocity and Force Diagram - Single Rotation Propellers.

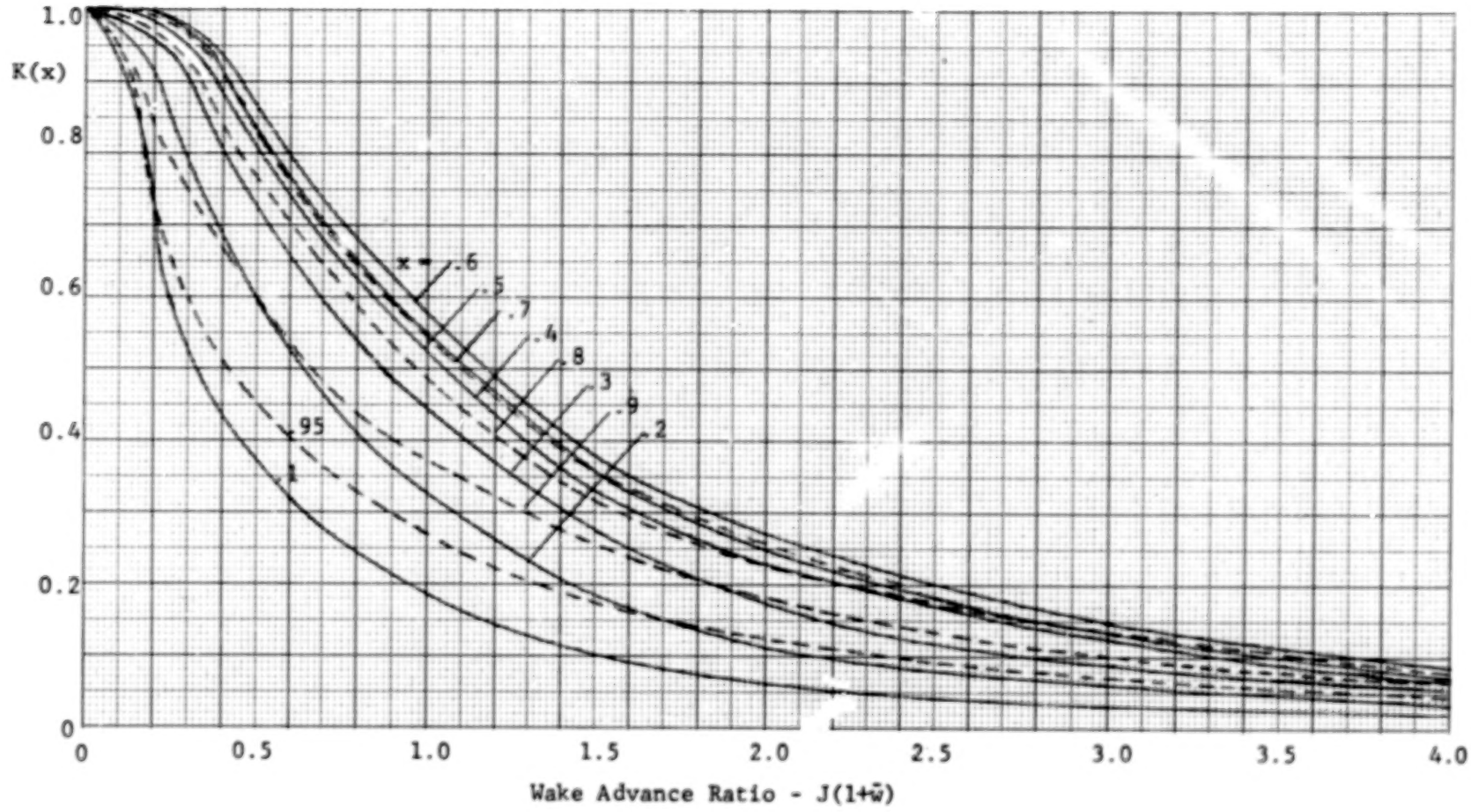

Figure 8. Circulation Function K(x) vs Wake Advance Ratio for a two-blade open propeller.

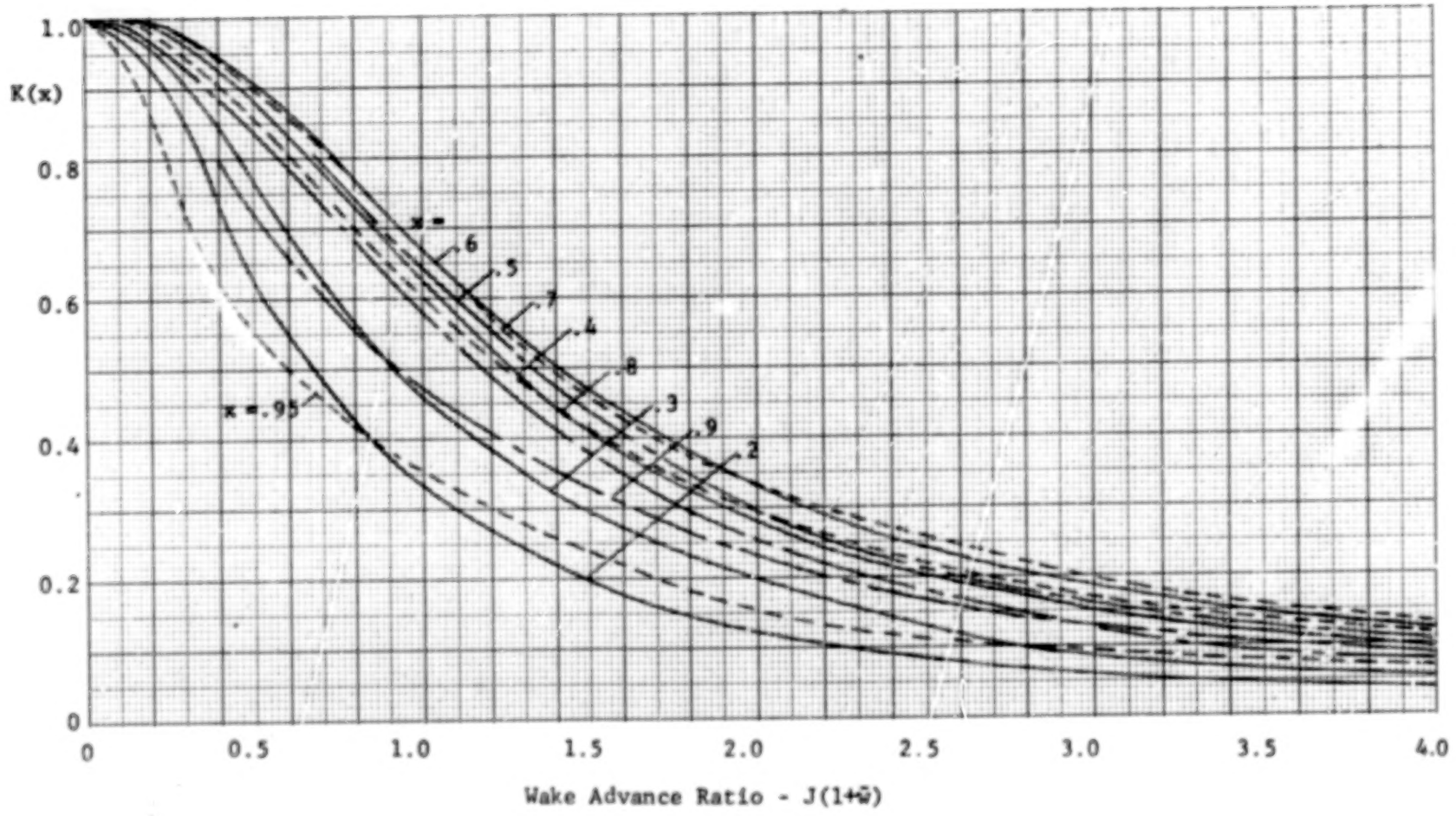

Figure 9. Circulation Function K(x) vs Wake Advance Ratio for a three-blade open propeller.

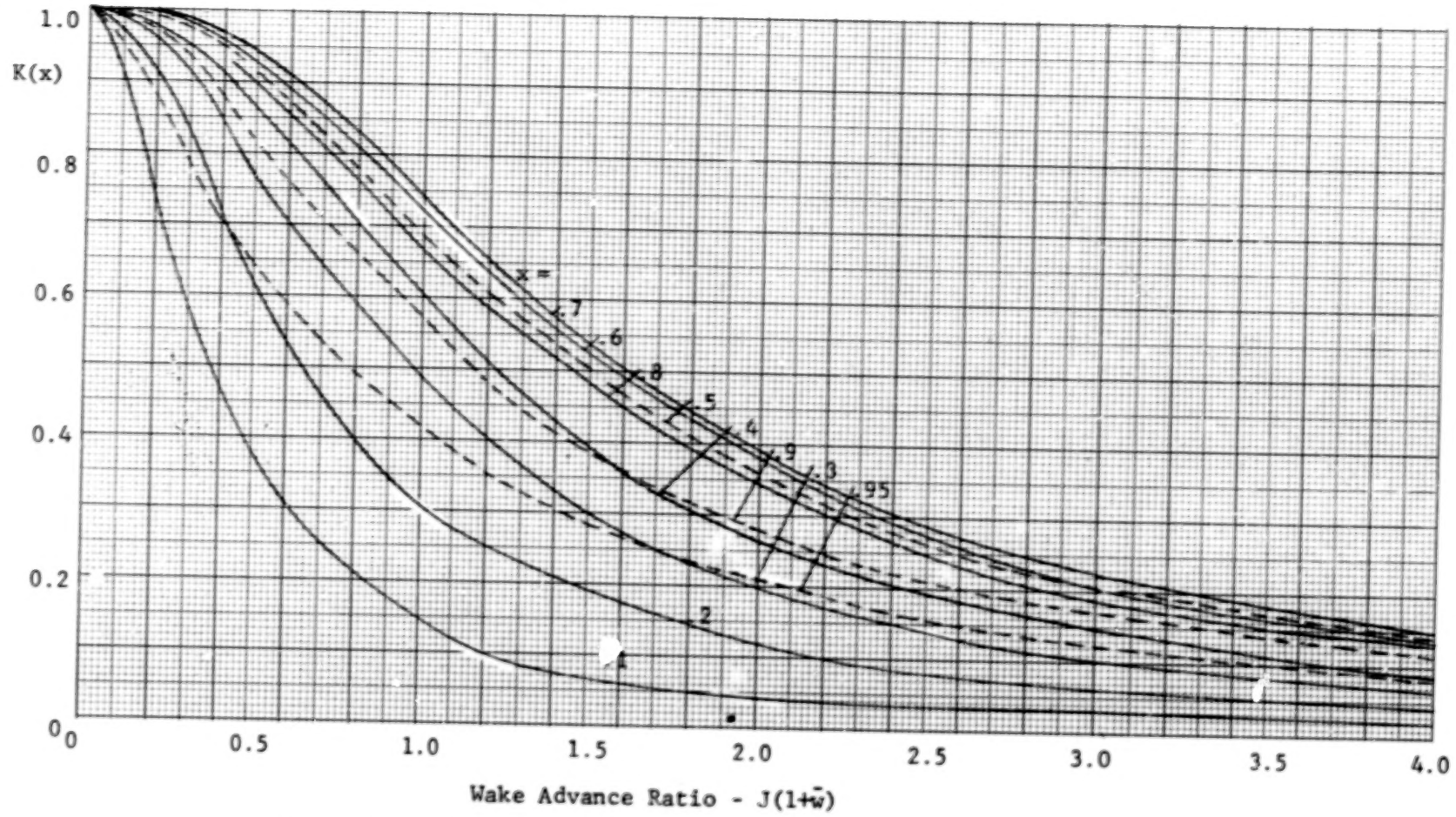

Figure 10. Circulation Function K(x) vs Wake Advance Ratio for a four-blade open propeller.

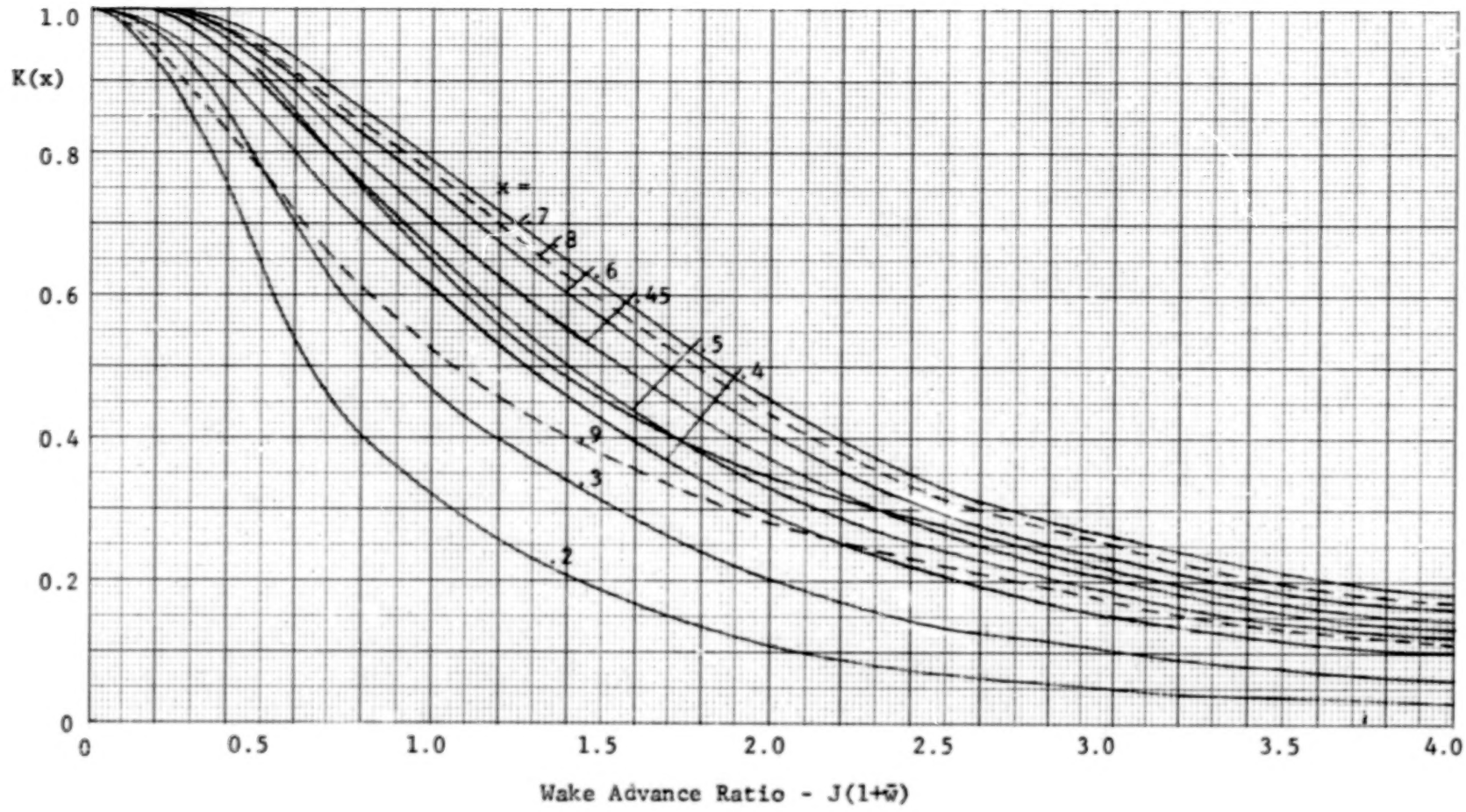

Figure 11. Circulation Function K(x) vs Wake Advance Ratio for a six-blade open propeller.

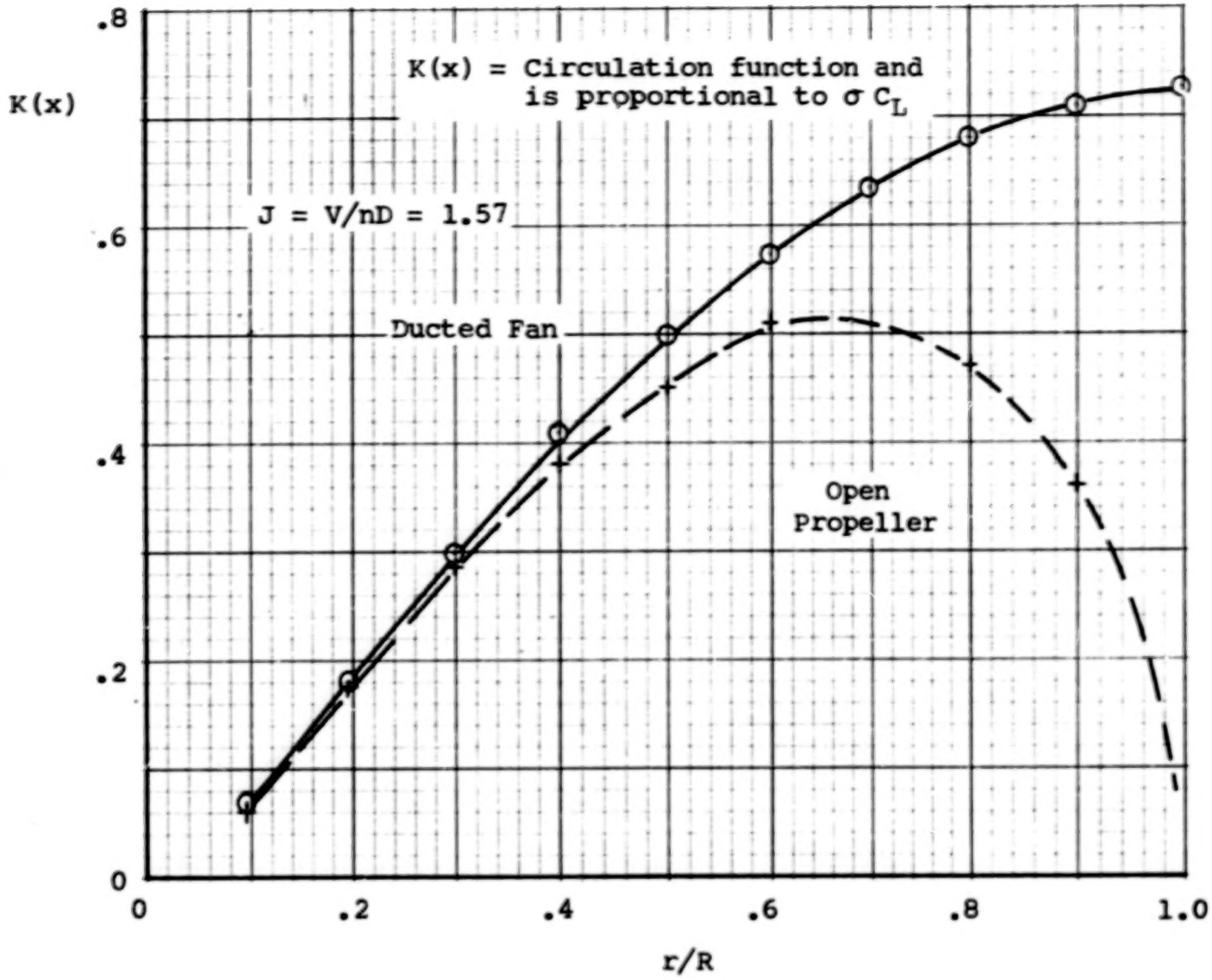

Figure 12. Comparison of the load distribution of a ducted fan and an open propeller.

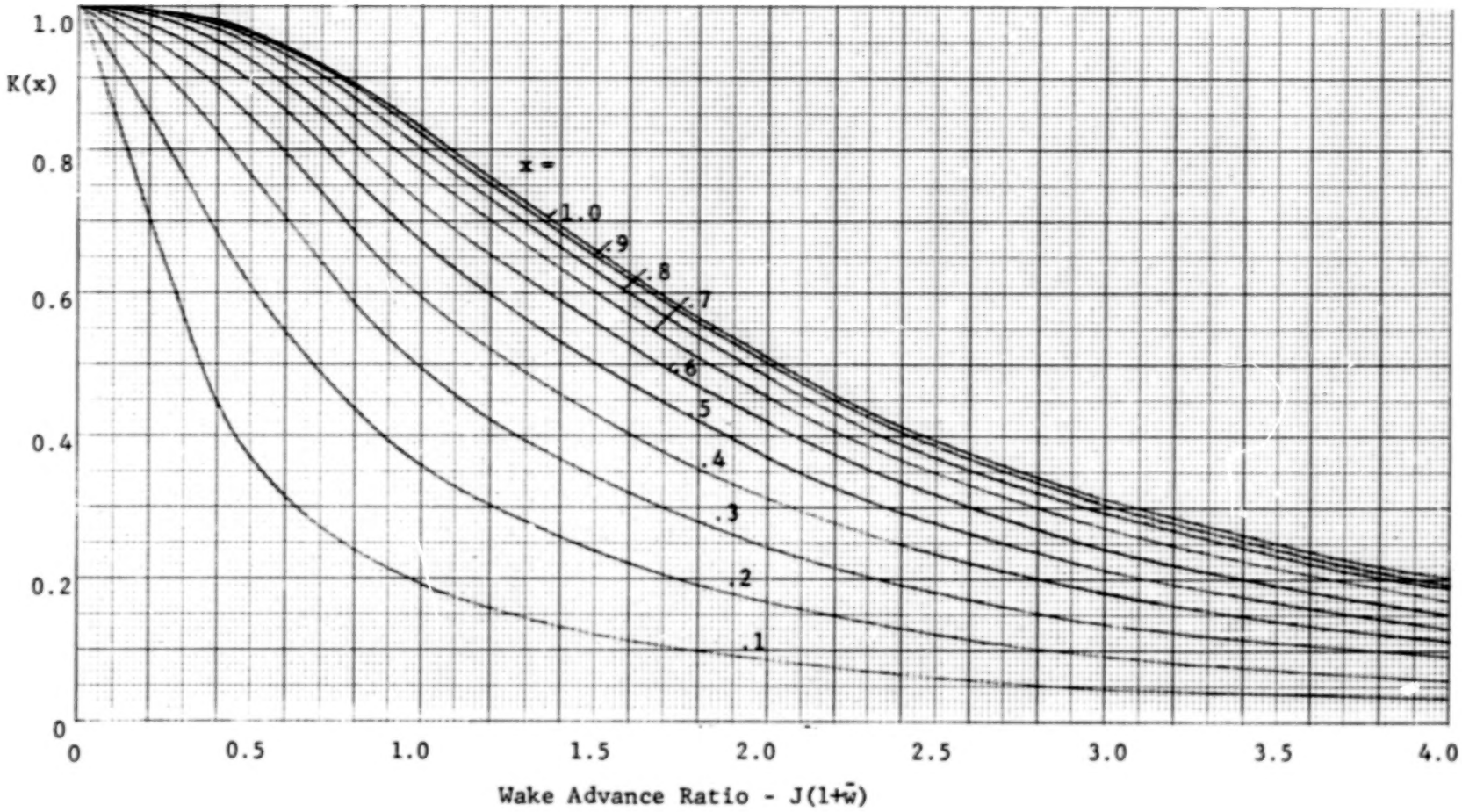

Figure 13. Circulation Function K(x) vs Wake Advance Ratio for a two-blade ducted propeller.

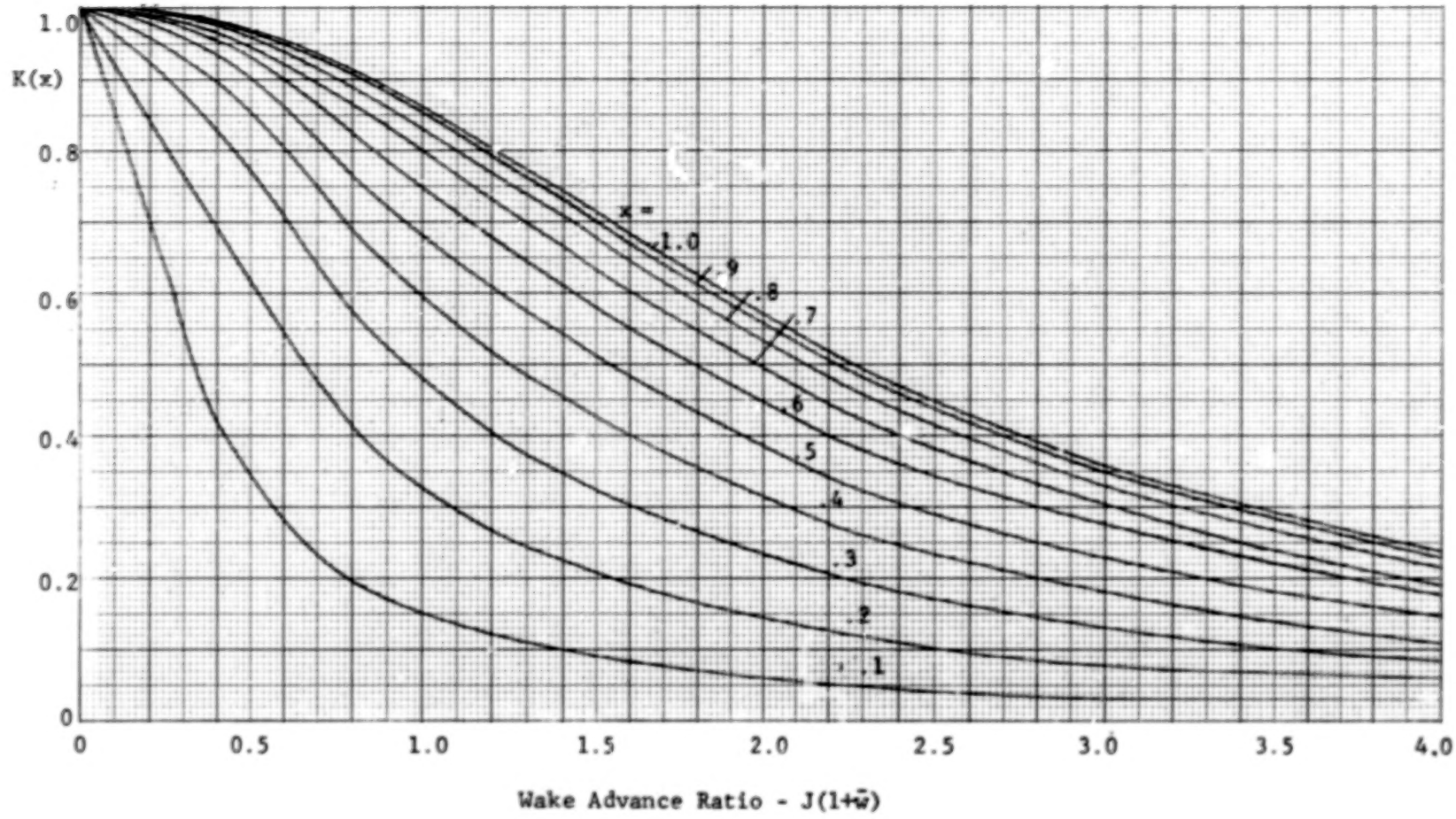

Figure 14. Circulation Function K(x) vs Wake Advance Ratio for a three-blade ducted propeller.

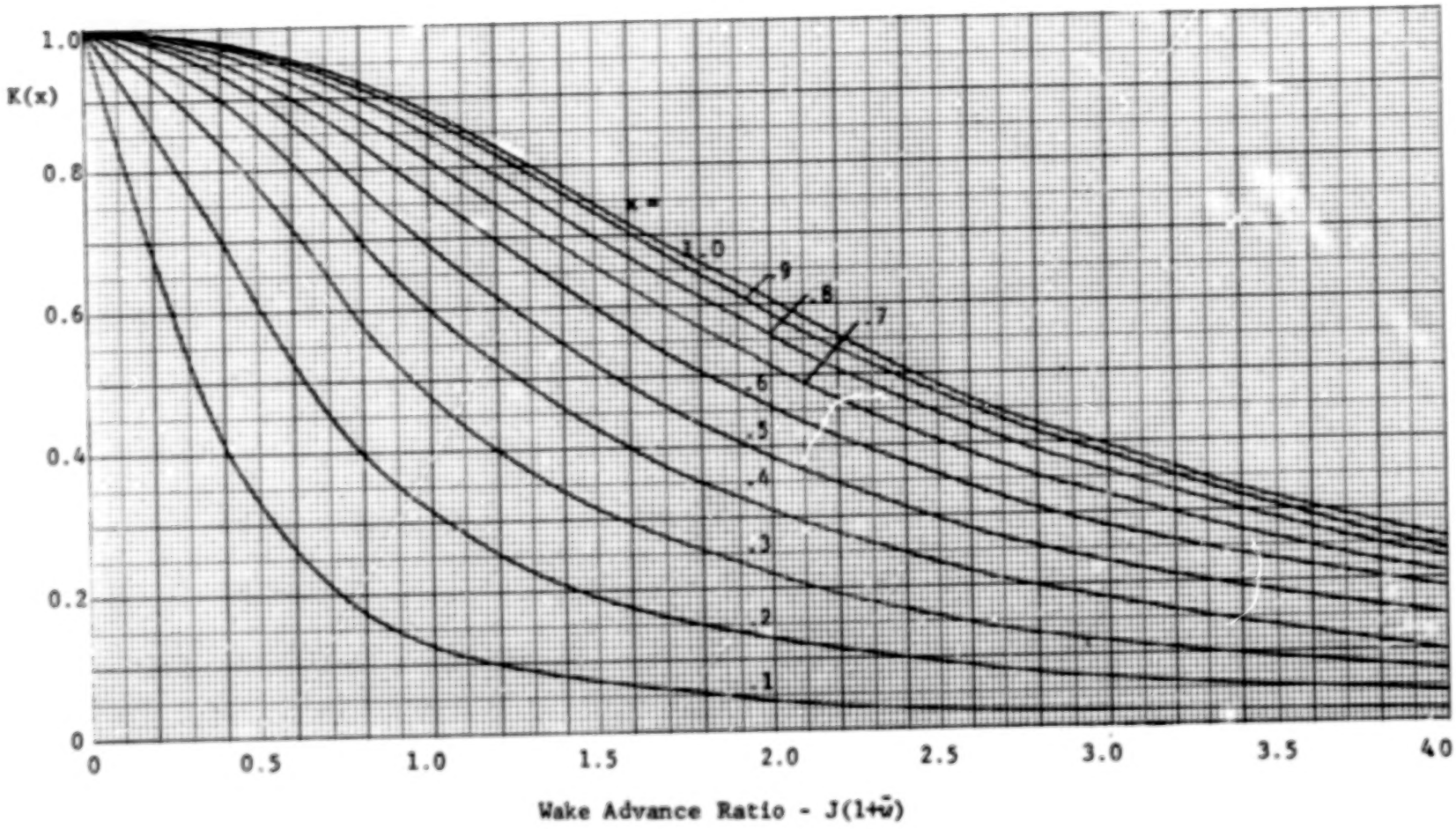

Figure 15. Circulation Function K(x) vs Wake Advance Ratio for a four-blade ducted propeller.

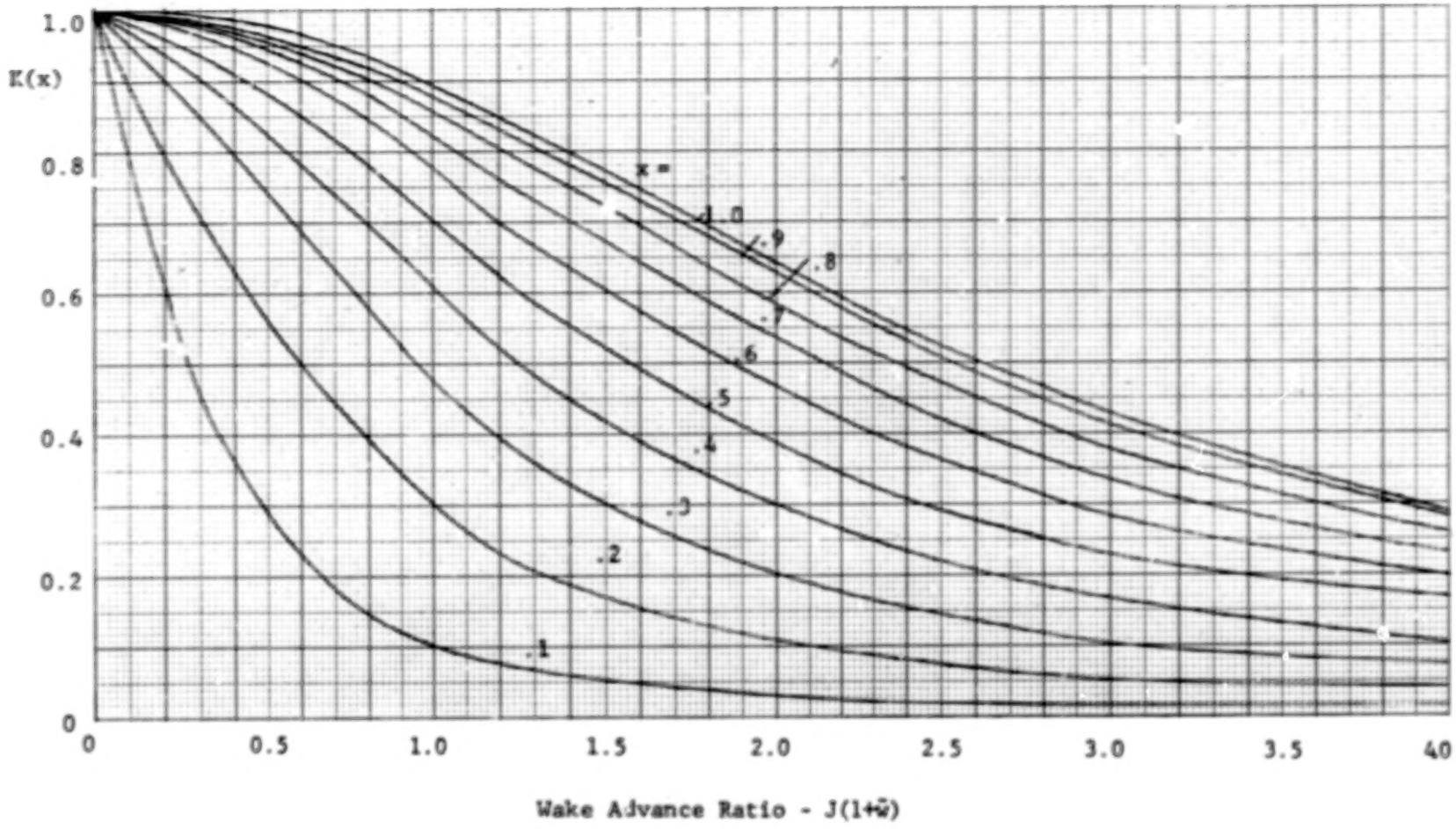

Figure 16. Circulation Function K(x) vs Wake Advance Ratio for a six-blade ducted propeller.

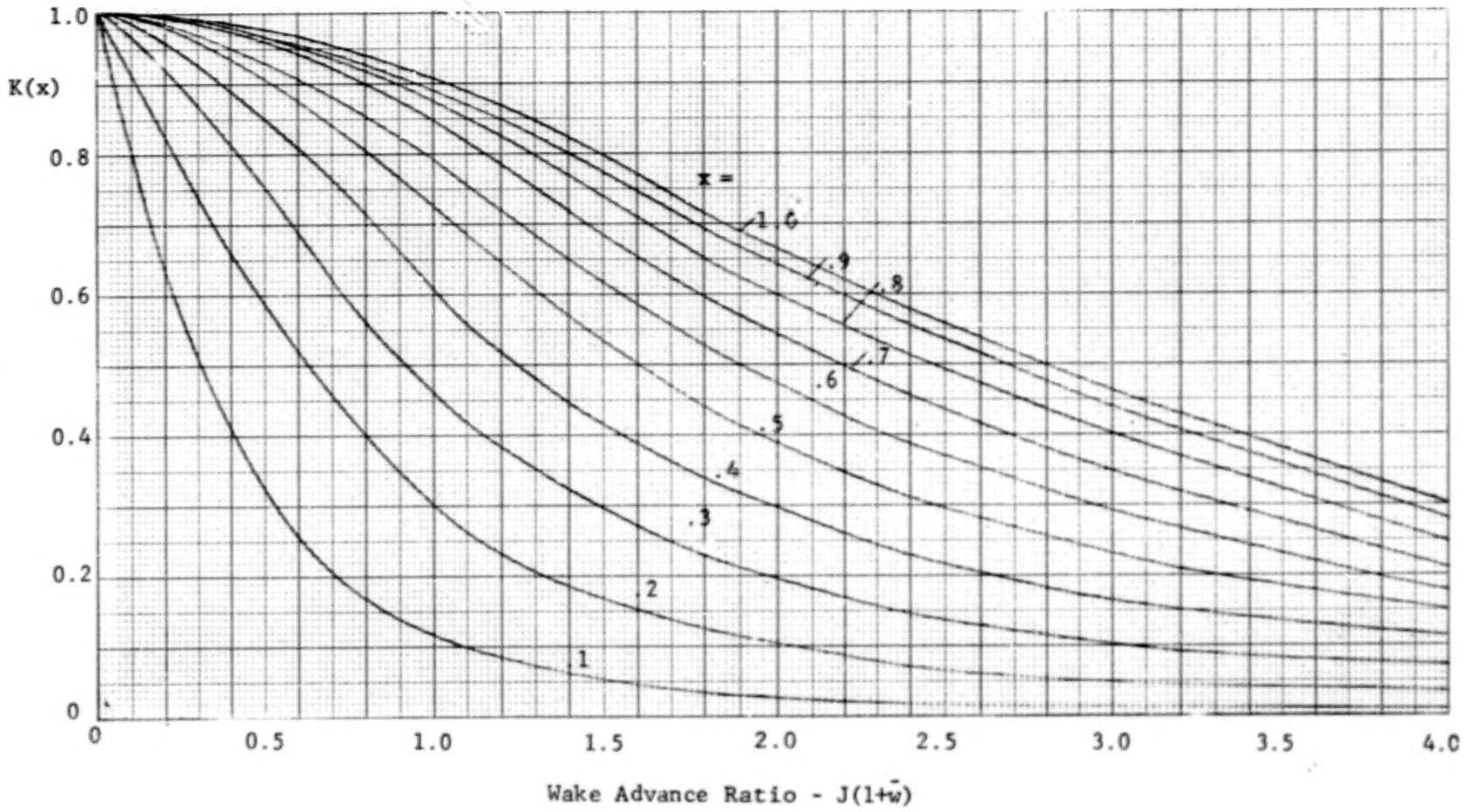

Figure 17. Circulation Function K(x) vs Wake Advance Ratio for an eight-blade ducted propeller.

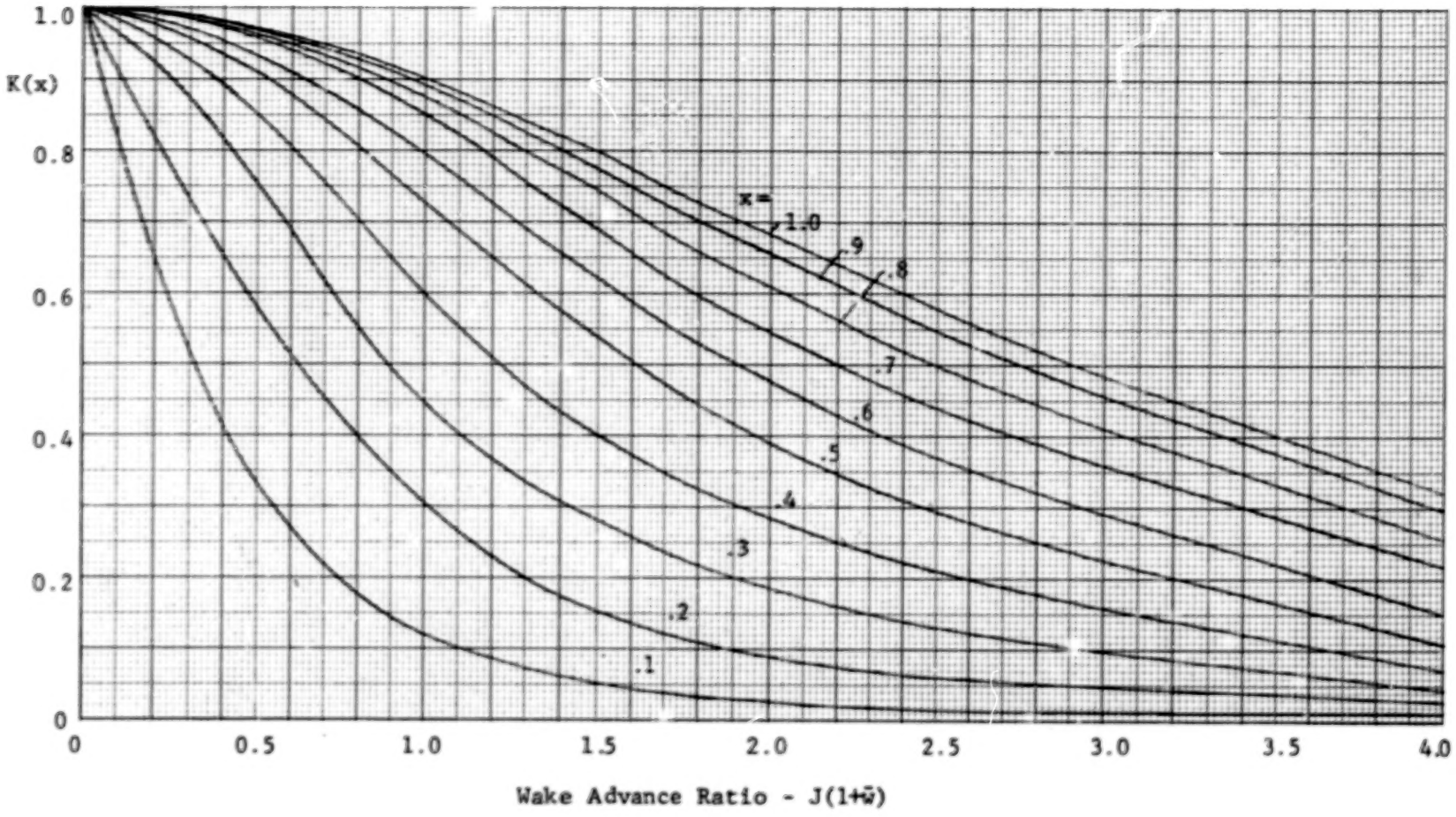

Figure 18. Circulation Function K(x) vs Wake Advance Ratio for a twelve-blade ducted propeller.

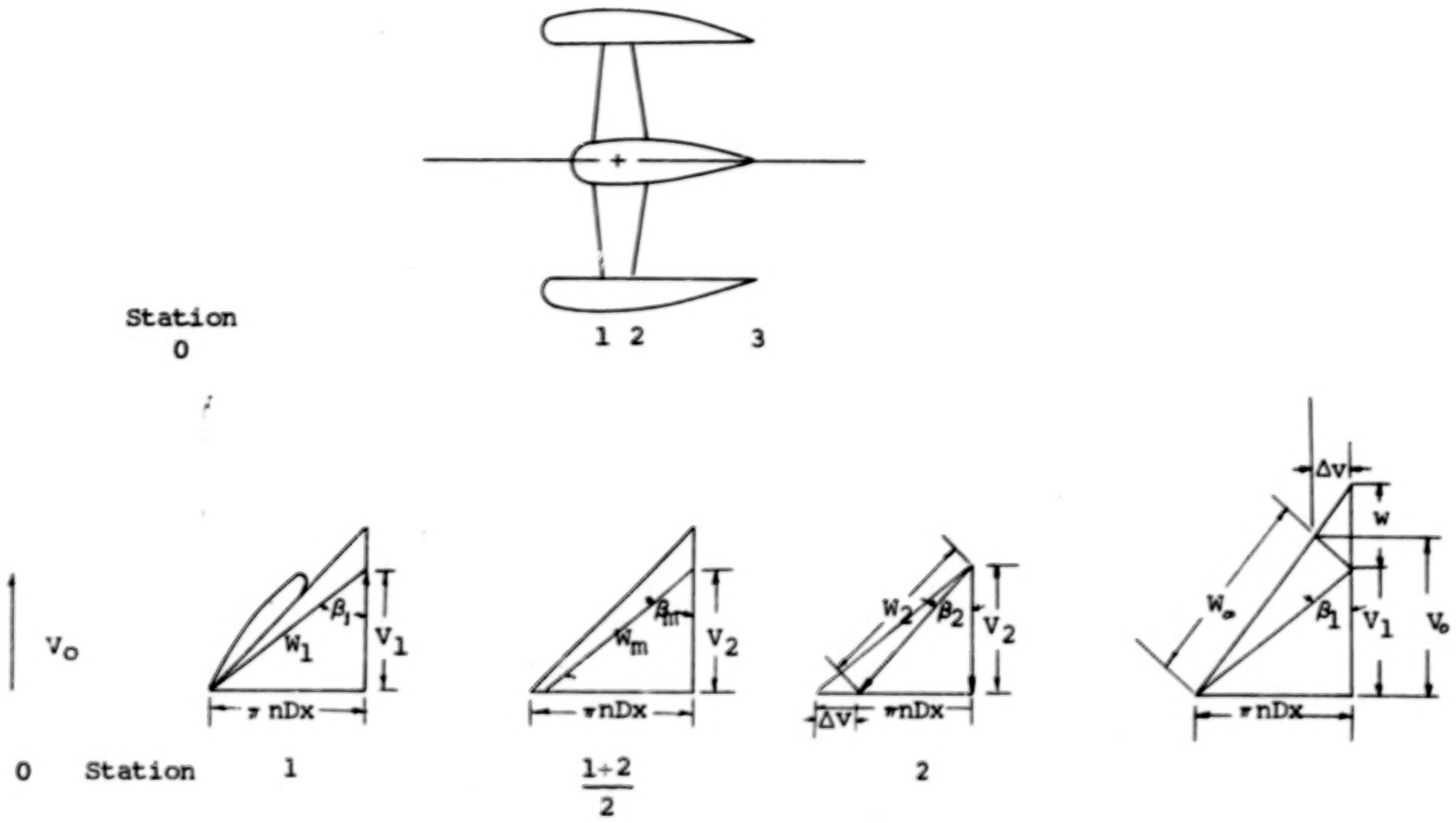

Figure 19. Velocity triangles for ducted fans.

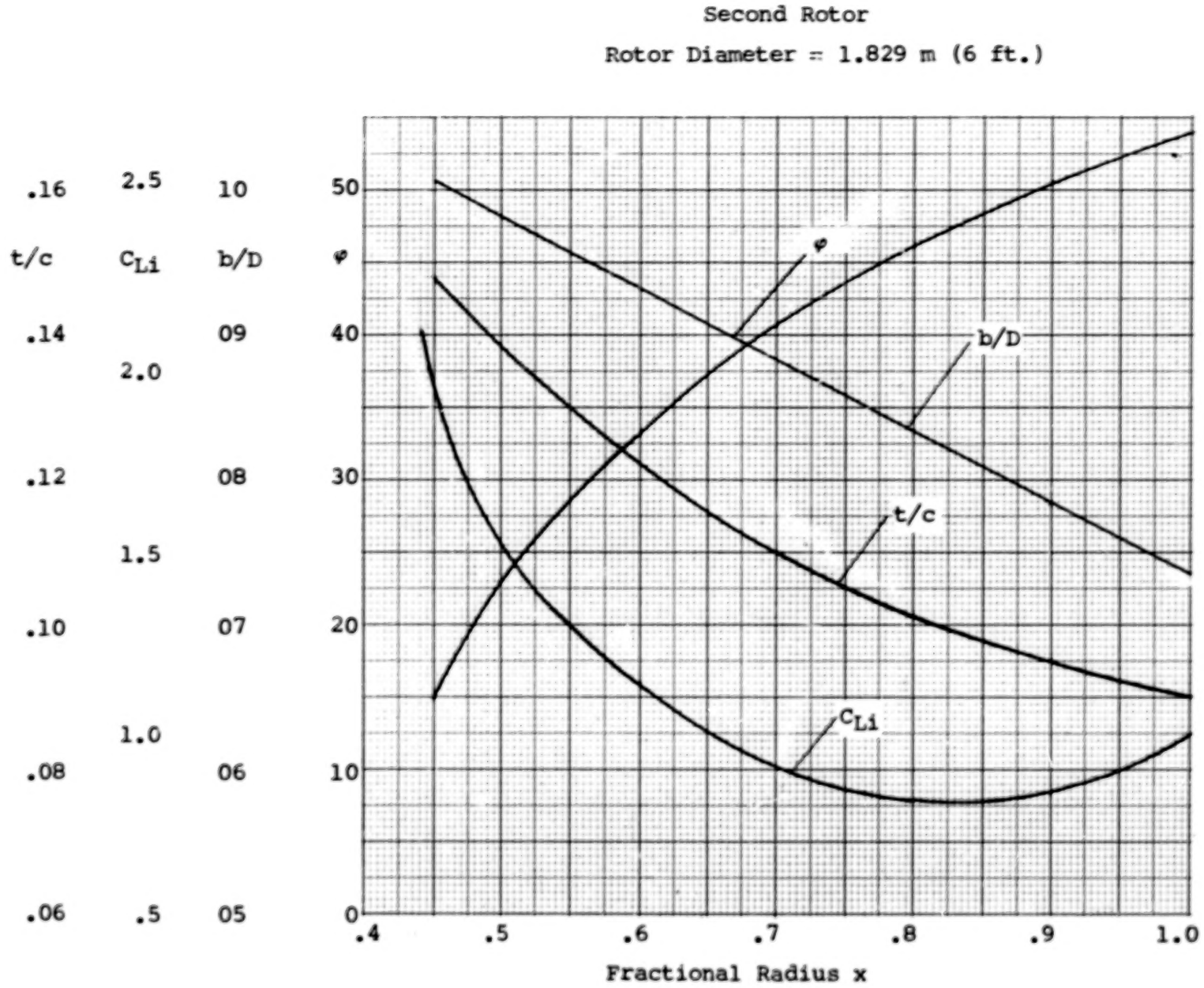

Figure 20. Blade Characteristics, Second Rotor.

END

June 27, 1979